②

AFOSR-TR. 88-1276
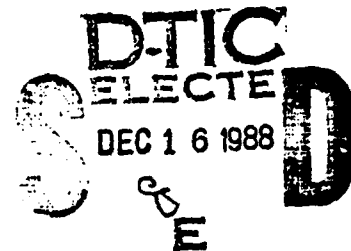
MULTIPLE TIME SCALE

METHODS AND GYROTRONS

FINAL REPORT

NOVEMBER 30, 1987

SAIC

Science Applications International Corporation

DTIC
ELECTE
DEC 1 6 1988
E

2

MULTIPLE TIME SCALE

METHODS AND GYROTRONS

FINAL REPORT

NOVEMBER 30, 1987

SAIC

Science Applications International Corporation

DTIC
ELECTE
DEC 1 6 1988
E

REPORT DOCUMENTATION PAGE

1a. REPORT SECURITY CLASSIFICATION	1b. RESTRICTIVE MARKINGS
UNCLASSIFIED	

2a. SECURITY CLASSIFICATION AUTHORITY	3. DISTRIBUTION / AVAILABILITY OF REPORT
	Approved for public release;
2b. DECLASSIFICATION / DOWNGRADING SCHEDULE	distribution is unlimited.

4. PERFORMING ORGANIZATION REPORT NUMBER(S)	5. MONITORING ORGANIZATION REPORT NUMBER(S)
	AFOSR·TR· 88-1276

6a. NAME OF PERFORMING ORGANIZATION	6b. OFFICE SYMBOL (If applicable)	7a. NAME OF MONITORING ORGANIZATION
Science Applications International Corp		AFOSR/NP

6c. ADDRESS (City, State, and ZIP Code)	7b. ADDRESS (City, State, and ZIP Code)
10260 Campus Point Drive San Diego, CA 92121	Building 410, Bolling AFB DC 20332-6448

8a. NAME OF FUNDING / SPONSORING ORGANIZATION	8b. OFFICE SYMBOL (If applicable)	9. PROCUREMENT INSTRUMENT IDENTIFICATION NUMBER
AFOSR	NP	F49620-86-C-0065

8c. ADDRESS (City, State, and ZIP Code)	10. SOURCE OF FUNDING NUMBERS			
	PROGRAM ELEMENT NO.	PROJECT NO.	TASK NO.	WORK UNIT ACCESSION NO.
Building 410, Bolling AFB DC 20332-6448	61102F	2301	A8	

11. TITLE (Include Security Classification)

(U) MULTIPLE TIME SCALE METHODS AND GYROTRONS

12. PERSONAL AUTHOR(S)
Menyuk, Vitello

13a. TYPE OF REPORT	13b. TIME COVERED	14. DATE OF REPORT (Year, Month, Day)	15. PAGE COUNT
FINAL	FROM 1 Jul 86 to 30 Sep 87	November 30, 1987	83

16. SUPPLEMENTARY NOTATION

17.	COSATI CODES		18. SUBJECT TERMS (Continue on reverse if necessary and identify by block number)
FIELD	GROUP	SUB-GROUP	
	20:09		
	20:03		

19. ABSTRACT (Continue on reverse if necessary and identify by block number)

This contract was terminated after only a single year because of the surprise departure of the PI from SAIC after only several months into the contract.

20. DISTRIBUTION / AVAILABILITY OF ABSTRACT	21. ABSTRACT SECURITY CLASSIFICATION
☒ UNCLASSIFIED/UNLIMITED ☒ SAME AS RPT. ☐ DTIC USERS	UNCLASSIFIED

22a. NAME OF RESPONSIBLE INDIVIDUAL	22b. TELEPHONE (Include Area Code)	22c. OFFICE SYMBOL
R J BARKER	(202) 767-5011	AFOSR/NP

DD FORM 1473, 84 MAR   83 APR edition may be used until exhausted.   SECURITY CLASSIFICATION OF THIS PAGE
All other editions are obsolete.

88 19

UNCLASSIFIED

REPORT DOCUMENTATION PAGE

1a. REPORT SECURITY CLASSIFICATION UNCLASSIFIED	1b. RESTRICTIVE MARKINGS
2a. SECURITY CLASSIFICATION AUTHORITY	3. DISTRIBUTION / AVAILABILITY OF REPORT Approved for public release;
2b. DECLASSIFICATION / DOWNGRADING SCHEDULE	distribution is unlimited.

4. PERFORMING ORGANIZATION REPORT NUMBER(S)	5. MONITORING ORGANIZATION REPORT NUMBER(S) AFOSR·TR· 88 - 1276

6a. NAME OF PERFORMING ORGANIZATION Science Applications International Corp	6b. OFFICE SYMBOL (If applicable)	7a. NAME OF MONITORING ORGANIZATION AFOSR/NP

6c. ADDRESS (City, State, and ZIP Code) 10260 Campus Point Drive San Diego, CA 92121	7b. ADDRESS (City, State, and ZIP Code) Building 410, Bolling AFB DC 20332-6448

8a. NAME OF FUNDING / SPONSORING ORGANIZATION AFOSR	8b. OFFICE SYMBOL (If applicable) NP	9. PROCUREMENT INSTRUMENT IDENTIFICATION NUMBER F49620-86-C-0065

8c. ADDRESS (City, State, and ZIP Code) Building 410, Bolling AFB DC 20332-6448	10. SOURCE OF FUNDING NUMBERS			

	PROGRAM ELEMENT NO.	PROJECT NO.	TASK NO.	WORK UNIT ACCESSION NO.
	61102F	2301	A8	

11. TITLE (Include Security Classification)

(U) MULTIPLE TIME SCALE METHODS AND GYROTRONS

12. PERSONAL AUTHOR(S)
Menyuk Vitello

13a. TYPE OF REPORT FINAL	13b. TIME COVERED FROM 1 Jul 86 to 30 Sep 87	14. DATE OF REPORT (Year, Month, Day) November 30, 1987	15. PAGE COUNT 83

16. SUPPLEMENTARY NOTATION

17.	COSATI CODES		18. SUBJECT TERMS (Continue on reverse if necessary and identify by block number)
FIELD	GROUP	SUB-GROUP	
	20:09 20:03		

19. ABSTRACT (Continue on reverse if necessary and identify by block number)

This contract was terminated after only a single year because of the surprise departure of the PI from SAIC after only several months into the contract.

20. DISTRIBUTION / AVAILABILITY OF ABSTRACT ☒ UNCLASSIFIED/UNLIMITED ☒ SAME AS RPT. ☐ DTIC USERS	21. ABSTRACT SECURITY CLASSIFICATION UNCLASSIFIED	
22a. NAME OF RESPONSIBLE INDIVIDUAL R J BARKER	22b. TELEPHONE (Include Area Code) (202) 767-5011	22c. OFFICE SYMBOL AFOSR/NP

DD FORM 1473, 84 MAR   83 APR edition may be used until exhausted.   SECURITY CLASSIFICATION OF THIS PAGE
All other editions are obsolete.

88 12

UNCLASSIFIED

MULTIPLE TIME SCALE METHODS AND GYROTRONS

FINAL REPORT

SUBMITTED TO

AIR FORCE OFFICE OF SCIENTIFIC RESEARCH
BOLLING AIR FORCE BASE
WASHINGTON, D.C. 20332
ATTENTION: DR. ROBERT BARKER

PREPARED BY

CURTIS R. MENYUK & PETER VITELLO

PLASMA PHYSICS DIVISION
SCIENCE APPLICATIONS INTERNATIONAL CORPORATION
1710 GOODRIDGE DRIVE
MCLEAN, VIRGINIA 22102 USA
(703) 734-4078

NOVEMBER 30, 1987

TABLE OF CONTENTS

I. INTRODUCTION

During the period of this program the scientific objectives were to complete a study of one-dimensional electrostatic plasmas using the discrete Hamiltonian method, and to construct a model of ridged high harmonic gyrotron oscillators using "standard" gyrotron modeling techniques. Ridged gyrotrons appear ideal for the future application of the multiple time scale, discrete Hamiltonian method. As with all gyrotrons, ridged gyrotrons are characterized by several primary time scales, which are the cyclotron period, the cavity RF field oscillation period, and the transit time through the gyrotron tube. If only one harmonic is being considered, then the cyclotron period and the cavity RF oscillation period need not be treated separately since only the difference between them has significance. For high harmonic emission, however, the ridged gyrotron appears to require the simultaneous treatment of multiple cyclotron harmonics and hence multiple harmonic time scales. In addition, mode competition, which can lead to coupling between multiple RF cavity modes, is possible and would also result in the need to treat several cavity frequencies simultaneously.

In investigating electrostatic plasmas, difference equations were obtained by integrating over unperturbed orbits, allow time steps much longer than the linear mode oscillation period. In our gyrotron modeling, we developed a detailed linear theory, and a nonlinear model using a non-interacting test particle approach to solving the electron guiding center coordinate system equations of motion in assumed cold cavity RF fields for ridged cavities. The ridged cavity systems which we studied have good potential for producing high frequency radiation from high harmonic emission. Our studies can be used to provide direct theoretical support for the ridged rectangular cavity experimental program being conducted by Ferendeci [1]. Two papers were submitted for journal publication during this contract period and one paper was presented at the Eleventh

International Conference on Infrared and Millimeter Waves. Copies of the papers are
given in the Appendices.

II. TECHNICAL REPORT

A. DISCRETE HAMILTONIAN METHOD

In order to test the discrete Hamiltonian method in relatively simple circumstances, Dr. Decyk and Dr. Menyuk studied one-dimensional electrostatic plasmas, which were either Maxwellian distributed or had a warm beam present. The discrete Hamiltonian method is predicated on two basic ideas: 1) By integrating over unperturbed orbits, it is possible to take time steps which are substantially longer than is possible using leapfrog codes which simply extrapolate linearly in phase space. 2) The equations of motion of a closed plasma (including electromagnetic interactions) are Hamiltonian. Therefore, by retaining this property in the discrete equations, one avoids certain nonlinear instabilities which can be very damaging to the long-term behavior of the system.

In principle, the discrete Hamiltonian equations can be written such that the discrete change in the particle spatial coordinate and momentum $\Delta \vec{x}$ and $\Delta \vec{p}$ depend on the *initial* value of $\vec{x}$ and the *final* value of $\vec{p}$. When integrating over the unperturbed orbits, we do not assume that the field is frozen, the assumption which is generally made in leapfrog codes. Instead, we assume that the waves vary according to the linear dispersion relation. This assumption allows us in principle to take time steps which are long compared to the linear mode oscillation period, but are short compared to the nonlinear time scale. Our formulation requires us to sum over the different linear modes in the system. In the one-dimensional, electrostatic problem which we have

3

studied, the discrete equations describing the particle push may be written as [2]

$$v^{n+1} - v^n = -\sum_k \frac{q\Phi_k^n}{m(v^{n+1} - \omega_k/k)} \left\{ \cos\left[kz^n + (kv^{n+1} - \omega_k)\tau + \phi_k^n\right] \right.$$

$$\left. - \cos\left(kz^n + \phi_k^n\right) \right\},$$

$$z^{n+1} - z^n = v^{n+1}\tau - \sum_k \frac{q\Phi_k^n}{m(v^{n+1} - \omega_k/k)^2} \left\{ \sin\left[kz^n + (kv^{n+1} - \omega_k)\tau + \phi_k^n\right] \right.$$

$$\left. - \sin\left(kz^n + \phi_k^n\right) - \left(kv^{n+1} - \omega_k\right)\tau\cos\left[kz^n + (kv^{n+1} - \omega_k)\tau + \phi_k^n\right] \right\},$$

$$(1)$$

where the superscript n indicates the time step, the subscript k indicates the mode number, and the ordinary variables k and ω are the wavenumber and frequency respectively. The variables τ, Φ_k^n, ϕ_k^n, and v_k give respectively the size of the time step, the mode potential, the mode phase, and the phase velocity. In the sum over k, we must distinguish between forward-going and backward-going waves. We do so by use of the particle current as well as the charge. Writing

$$C^\pm = \left(k^2/4\pi\right)\Phi_{\pm k}\cos\left(-\omega_{\pm k}\tau + \phi_{\pm k}\right),$$

$$S^\pm = \left(k^2/4\pi\right)\Phi_{\pm k}\sin\left(-\omega_{\pm k}\tau + \phi_{\pm k}\right),$$

$$(2)$$

we find

$$C^+ = (1/2)(\rho_{kr} + kj_{kr}/\omega_k), \qquad C^- = (1/2)(\rho_{kr} - kj_{kr}/\omega_k),$$

$$S^+ = (1/2)(\rho_{ki} - kj_{ki}/\omega_k), \qquad S^- = (1/2)(\rho_{ki} + kj_{ki}/\omega_k),$$

$$(3)$$

where $+$ and $-$ indicate respectively the forward-going and backward-going waves while the subscripts r and i indicate the real and imaginary parts of the charge and current in the usual Fourier decomposition.

Equations (1–3) are only weakly implicit; that is to say that the discrete equation depends on the field at the beginning of the time step. As a consequence, one can solve for the change in z and v directly for each particle using Newton's method.

4

It is natural to inquire whether the lack of time-centering of the fields which this represents has any bad effects. It is possible, in fact to write down a strongly implicit form of (1) which is time-centered and strongly implicit

$$v^{n+1} - v^n = -\sum_k \left\{ \frac{q\Phi_k^{n+1}}{m(v^{n+1} - \omega_k/k)} \cos\left[kz^n + \left(kv^{n+1} - \omega_k\right)\tau + \phi_k^{n+1}\right]\right.$$

$$\left. - \frac{q\Phi_k^n}{m(v^{n+1} - \omega_k/k)} \cos\left(kz^n + \phi_k^n\right) \right\},$$

$$z^{n+1} - z^n = v^{n+1}\tau - \sum_k \left(\frac{q\Phi_k^{n+1}}{mk(v^{n+1} - \omega_k/k)^2} \left\{ \sin\left[kz^n + \left(kv^{n+1} - \omega_k\right)\tau + \phi_k^{n+1}\right] \right. \right.$$

$$\left. - \left(kv^{n+1} - \omega_k\right)\tau\cos\left[kz^n + \left(kv^{n+1} - \omega_k\right)\tau + \phi_k^{n+1}\right] \right\}$$

$$\left. - \frac{q\Phi_k^n}{m(v^{n+1} - \omega_k/k)^2} \sin\left(kz^n - \phi_k^n\right) \right).$$

$$(4)$$

The linear dispersion relation which results from (4) agrees *exactly* with the linear dispersion relation obtained by solving the continuous, exact equations of motion, in contrast to (1) which has small differences. We tried solving (4) using a predictor-corrector approach. Remarkably, however, this approach did not converge. We will return to the reason for this later. As a consequence of this non-convergence, we always used (1) in practice.

The first problem we faced in solving these equations is that calculating all of the sine and cosine functions in (1) for each of the modes proved to be prohibitively expensive even for a restricted number of modes (16 or 32 in practice). To deal with this difficulty, we wrote the code, including the Newton's method iteration, to take advantage of vectorization on the CRAY computers (where we ran our code) and also to make maximum use of recursion relations. Through the use of these relations, it is possible to reduce the number of cosine and sine evaluations to one each per particle per time step. With these changes, each time step in our code was a factor of 5 longer than

in an optimized leapfrog code. Thus, the crossover point to obtain computational time saving occurs when $\omega_{pe}\tau \simeq 1$, a value which we regularly exceeded in our calculations.

Menyuk and Decyk [3] have already reported that when modes are present with phase velocities in the bulk of the plasma, the discrete Hamiltonian approach is strongly unstable. The reason is that the wave amplitudes fluctuate rapidly on a time scale about equal to ω_{pe}^{-1} and the code cannot follow these fluctuations since they violate the assumption that wave amplitudes change slowly on the linear time scale. While the fluctuations are due to the use of discrete particles, little improvement is obtained in a thermal simulation plasma by increasing the number of particles. The time scale of the fluctuations scales like the trapping times in the individual k-modes, $\tau_{fluct} \propto E_k^{-1/2}$, and $E_k \propto N^{-1/2}$, where N is the number of particles. Hence, $\tau_{fluct} \propto N^{-1/4}$ and increases only weakly with N. Our constraint is $\tau < \tau_{fluct}$ for stability. We have verified that increasing the number of particles in our simulation by a factor 16 allows approximately double the size of τ before the strong instability sets in. When it is present, it occurs on a time scale $\omega_{pe}T \simeq 10$–20 for the cases we ran, where T is the total run time.

During this contract period, we also found a new source of numerical instability which occurs on a very long time scale, $\omega_{pe}T \simeq 300$ when $\omega_{pe}\tau = 4$ and $\omega_{pe}T \simeq 400$ when $\omega_{pe}\tau = 3$. This instability and its effect on phase space is shown in Figure 1 in the case $\omega_{pe}\tau = 3$. We at first thought that this problem was due to the lack of time centering in the fields, but, as previously noted, taking predictor-corrector steps to center the fields did not converge and thus only exacerbated the problem. The real culprit turned out to be rapid fluctuations in the field amplitudes due to the random particle assortment which *still* occurs even when the waves' phase velocities are outside the bulk plasma. Indeed, these rapid fluctuations also account for the failure of the predictor-corrector scheme to converge. To deal with this difficulty effectively, it is necessary to use quiet start techniques [4]. The dramatic improvement which results

6

can be seen by comparing Figure 2 with Figure 1. It should be noted, however, that the use of quiet start techniques is not a solution over indefinitely long times. At $\omega_{pe}T = 450$, the particles have clearly been randomized. On a longer time scale, we anticipate that the plasma will once more be numerically unstable. This problem can in principle be eliminated by periodic regridding [4]. We have not, however, explored this question ourselves, feeling that this instability occurs on such a long time scale that it is unlikely to be of interest in most cases.

Finally, we have studied the beam-plasma instability, using a 10%, a 1%, and a 0.1% beam. The beam amplitude is lowered by decreasing q and m for each particle in the beam, holding q/m constant, rather that by decreasing the number of particles, in order to obtain a reasonable beam resolution. The phase space evolution is shown in Figure 3 for the 10% beam. The trapping and thermalization of the beam is readily apparent. In Figure 4, we show the evolution of the field energy for the three different amplitude beams. As expected, the instability becomes less energetic when going from a 10% beam to a 1% beam, and disappears for a 0.1% beam. These results are consistent with the results of a comparison leapfrog code which we have run.

We conclude that while the discrete Hamiltonian method is not simple to implement in practice, it can be useful in situations where the number of modes needed is small and long time steps are required.

B. DEVELOPMENT OF GYROTRON MODELING TOOLS

The first stage in the implementation of the discrete Hamiltonian method to gyrotron modeling is the choice of a device to study and the development of a set of basic gyrotron models, based upon conventional approximations and techniques, which can be modified and expanded upon. As initial devices to investigate, we have chosen a high harmonic ridged rectangular cavity and a ridged co-axial cylindrical cavity gyrotron oscillator. The cavity cross sections for the two devices are shown in Figures 5a and 5b. The emission harmonics are defined by $s\Omega/\gamma = \omega$, where ω is the cavity frequency and s is the harmonic number. As emission for the gyrotron occurs at harmonics of the electron cyclotron frequency, high frequency emission implies either the use of large magnetic fields or high harmonic operation. If frequencies as high as the millimeter wave regime are to be achieved using conventional magnets, one must use third and higher harmonics. Studies of gyrotrons with ridged rectangular tubes [1, 5–9] and ridged cylindrical tubes [10–18] indicate that the ridged cavity structure provides an excellent high harmonic interaction and good mode selection.

To aid us in our understanding of ridged gyrotron oscillators, we have developed a detailed linear theory for the interaction between the electron beam and cavity RF field. Our model treats gyrotrons with ridged cross-sections whose basic symmetry is either rectangular or cylindrical. The model calculates the start-oscillation condition, QP_b, where Q is the cavity Quality factor and P_b is the initial beam power. The start-oscillation condition determines the beam power at which a cavity will oscillate and is needed both for an oscillator design and to investigate mode competition. The linear model also solves for the shift in the cavity resonance frequency ω caused by the presence of the electron beam. It provides an excellent basis for benchmarking our nonlinear codes, and is also an aid in the design of an optimum high harmonic ridged

8

cavity gyrotron. Details of the model are given in the Appendices which contains papers which have been submitted for journal publication.

With our linear model in hand, we turned to the ridged rectangular gyro-TWT amplifier work of Ferendeci and Han [1, 5–8] and the ridged cylindrical gyrotron oscillator modeling of Chu and Dialetis [14–15] to begin a program of investigation of ridged cavities. A comparison of our modeling of the ridged cavity RF field with that of Ferendeci and Han revealed that while there was exact agreement between our approach and the basic equations describing the RF field, the solutions for several of the resonant frequencies differed. Upon a careful examination of the RF field described in Han's PhD thesis [5], we have concluded that extraneous terms had been included by Han in the solution of the cavity frequency dispersion relation. For the TE_{02} mode which Ferendeci and Han believed to be optimal for their design, no discrepancies exist with our calculations.

We find, in agreement with Ferendeci and Han, that the addition of ridges greatly enhances the interaction between the electron beam and the RF field at high harmonics. Figure 6 shows the TE_{021} start oscillation condition as a function of magnetic field B_o for a smooth walled rectangular cavity suggested by Ferendeci and Han. See Figure 5b. The electron beam is placed in the center of the cavity to allow as large a Larmor radius as possible. For the smooth walled cavity and the chosen beam position, there is emission only at even harmonics. With increasing harmonic number the gyrotron interaction rapidly weakens, and the required start oscillation condition increases. The addition of ridges to the cavity creates strong fringe fields about the ridge openings as is evident from Figure 7. These fringe fields lead to a strong high harmonic emission. In Figure 8, we show the result that adding ridges has upon the start oscillation condition. The gyrotron emission interaction now occurs at all cyclotron harmonics. The high harmonic start oscillation condition is very low, and even *decreases* with increasing harmonic number. Ferendeci and Han [1, 5–8] did not analyze their equations and

9

did not find this effect. Harmonics greater than 6 for the TE_{021} mode have Larmor radii which would cause the beam electrons to strike the cavity wall and thus are not included in the figure.

Modes other than the TE_{021} mode may be excited by the electron beam. In Figure 9 we show the start oscillation condition for the modes TE_{mn1} where $m = 0, 1, 2$ and $n = 1, 2, 3, 4, 5$. What is evident from this figure is that other modes have high harmonic resonances with start oscillation conditions smaller that that of the sixth harmonic of TE_{021}. Also, the harmonic emission resonances of TE_{021} are likely to suffer from mode competition from the other strong emission resonances. As our treatment of the RF cavity field modes is approximate (only one expansion term is used in the ridges) the cavity frequencies for the modes and therefore the values of the background magnetic field for the harmonic resonances cannot be exactly determined from our present theory. The relative positions of the harmonics in Figure 9 should therefore be taken as an indication of possible mode competition and not a definitive statement as to where it will exist.

Start oscillation calculations were conducted for the ridged cylindrical cavity as well. In Figure 10 we show for an axis encircling beam how the presence of the ridges can greatly reduce the value of QP_b. We found that our model agrees with the value of QP_b calculated for the electron cyclotron maser interaction by Chu and Dialetis [14-15]. However, Chu and Dialetis did not include the peniotron resonance in their modeling. The peniotron interaction, which can lead to a very high peak efficiency [19], is always present in gyrotron devices along with the standard electron cyclotron maser interaction. As the peniotron interaction was actually the stronger interaction over much of the parameter space considered by Chu and Dialetis, the values given in their paper for the minimum start oscillation condition are not correct.

In addition to the linear, ridged model, we have also developed a nonlinear, ridged gyrotron model. The nonlinear model uses a non-interacting test particle approach to

10

solving the electron equation of motion

$$\frac{d\vec{U}}{dz} = -\frac{\gamma}{U_s}\left[\vec{E} + \frac{\vec{U} \times \vec{B}}{\gamma}\right],\tag{5}$$

using the assumed cold cavity RF fields. (See the Appendices for a description of the ridged cavity fields.) In (5) $\vec{U}$ is the dimensionless momentum vector, $\vec{U} = \gamma\vec{\beta}$, where γ give the particle energy and β is the velocity in terms of the speed of light. Dimensionless units scaled to the cavity length R are used in the modeling so that the results are able to be scaled to any frequency cavity. The nonlinear code uses the standard gyrotron modeling approach in that the RF field in expanded in terms of the cyclotron harmonics in an infinite sine-Bessel series about the electron guiding center. In the code, this sum is truncated to a small set of terms, typically 3–10. If only one harmonic expansion term is dominant, then using the fact that $(\omega - s\Omega/\gamma)t \ll \omega t$, a slow time scale treatment can be used to take time steps much larger that the cyclotron period. Comparison in the weak field limit has shown good agreement between the linear theory and the nonlinear model.

III. REFERENCES

[1] A.M. Ferendeci and C.C. Han, "High Energy Dense Ribbon Beams and High Harmonic Gyrotron at Millimeter Wavelengths," (Proposal submitted to AFOSR).

[2] C.R. Menyuk, *Physica,* vol. 11D, 109 (1984).

[3] C.R. Menyuk & V.K. Decyk, "Discrete Hamiltonian Plasma Simulations," *11th Conf. on the Numerical Simulation of Plasmas,* Montreal, Canada (June, 1985).

[4] Y. Matsuda & F.W. Crawford, *Phys. Fluids,* vol. 18, 1336 (1975).

[5] C.C. Han, "High Harmonic Rectangular Gyrotron," Ph.D. thesis, Case Western Reserve University (1984).

[6] A.M. Ferendeci & C.C. Han, "Theory of high harmonic rectangular gyrotron for TE_{mn} modes," *IEEE Trans. Electron Devices,* vol. ED-31, pp. 1212–1218 (1984).

[7] C.C. Han & A.M. Ferendeci, "Nonlinear analysis of a high harmonic rectangular gyrotron," *Int. J. Electron.,* vol. 57, pp. 1055–1063 (1984).

[8] A.M. Ferendeci and C.C. Han, "Linear Analysis of an Axially Grooved Rectangular Gyrotron for Harmonic Operation," *Int. J. Infrared Millimeter Waves,* vol. 6, pp. 1267–1283 (1985).

[9] Q.F. Li & J.L. Hirshfield, "Gyrotron traveling wave amplifier with out-ridged waveguide," *Int. J. Infrared Millimeter Waves,* vol. 7, pp. 71–98 (1986).

[10] Y.Y. Lau & L.R. Barnett, "Theory of a low harmonic field gyrotron (Gyromagnetron)," *Int. J. Infrared Millimeter Waves,* vol. 3, pp. 619–744 (1982).

[11] P.S. Rha, L.R. Barnett, J.M. Baird, & R.W. Grow, *Int. Electron Device Meet.,* pp. 525–538 (1985).

[12] R.W. Grow & U.A. Shrivastava, "Impedance calculations for traveling wave gyrotrons operating at harmonics of the cyclotron frequency in magnetron-type circuits operating at the PI mode," *Int. Electron Devices Meet.,* pp. 384–387 (1982).

[13] H.S. Uhm, C.M. Kim, & W. Namkung, "Linear theory of cusptron microwave tubes," *Phys. Fluids*, vol. 27, pp. 488–498 (1984).

[14] K.R. Chu & D. Dialetis, "Theory of harmonic gyrotron oscillator with slotted resonant structure," *Int. J. Infrared Millimeter Waves*, vol. 5, pp. 37–55 (1984).

[15] K.R. Chu & D. Dialetis, "Kinetic theory of harmonic gyrotron oscillator with slotted resonant structure," *Infrared Millimeter Waves*, vol. 13, pp. 45–74 (1985).

[16] W. Namkung & J.Y. Choe, "Experimental results of cusptron microwave tube study," *IEEE Trans. Nuclear Sci.*, vol. NS-32, pp. 2885–2887 (1985).

[17] U.A. Shrivastava, R.W. Grow, P.S. Rha, J.M. Baird, & L.R. Barnett, "Threshold power transfer and the gyrotron and peniotron oscillators operating at the harmonic cyclotron frequencies using coaxial electron beam-circuit configurations," *Int. J. Electron.*, vol. 61, pp. 33–59 (1986).

[18] P. Vitello, *Eleventh International Conf. Infrared Millimeter Waves*, pp. Tirrenia, Pisa, Italy, 46–48 (1986).

[19] P. Vitello & K. Ko, "Mode competition in the gyro-peniotron oscillator," *IEEE Trans. Plasma Sci.*, vol. PS-13, pp. 454–463 (1985).

IV. FIGURES

Figure 1. Development of the weak numerical instability due to wave amplitude fluctuations $(\omega_{pe}\tau = 3$, $N = 40{,}000$, $n_{mode} = 16)$. a) $\omega_{pe}T = 300$, b) $\omega_{pe}T = 450$, c) field energy vs. time.

Figure 2. Effect of a quiet start on the weak numerical instability (same parameters as in Figure 1). a) $\omega_{pe}T = 0$, b) $\omega_{pe}T = 450$, c) field energy vs. time. Note at $T = 0$, the regular pattern characteristic of quiet start simulations.

Figure 3. Phase space plots of the beam-plasma instability (10% beam, $N_{total} = 32{,}000$, $N_{beam} = 3{,}200$, $\omega_{pe}\tau = 2$, $n_{mode} = 16$). a) $\omega_{pe}T = 0$, b) $\omega_{pe}T = 50$, c) $\omega_{pe}T = 100$.

Figure 4. Field energy vs. time. a) 10% beam, b) 1% beam, c) 0.1% beam.

Figure 5a. Cross-section of the ridged cylindrical gyrotron.

Figure 5b. Cross-section of the ridged rectangular gyrotron.

Figure 6. TE_{021} mode start oscillation condition for a smooth walled rectangular cavity for an electron beam with energy 72 keV and $\beta_z = 0.28$. The cavity parameters are $L_x = 2.1987R$ and $L_z = 15R$. The resonances are labeled by their harmonic number.

Figure 7. E_z RF field for a ridged rectangular cavity with $L_x = 2.1987R$, $R_o = 1.1983R$, $w = 0.05455R$, and $N = 3$.

Figure 8. TE_{021} mode start oscillation condition for a the ridged rectangular cavity for an electron beam with 72 keV and $\beta_z = 0.28$. The resonances are labeled by their harmonic number.

Figure 9. TE_{mn1} mode start oscillation condition for a the ridged rectangular cavity for an electron beam with 72 keV and $\beta_z = 0.28$. All modes with $m = 0, 1, 2$ and $n = 1, 2, 3, 4, 5$ are shown. The arrow shows the TE_{021} 6th harmonic emission resonance.

Figure 10. Variation of the start oscillation condition for the third harmonic electron cyclotron maser interaction (solid curves) and second harmonic peniotron interac-

14

tion (dashed curves) as a function of d/a for the TE_{311} mode. Note that in the notation used here that $d/a = R_o/R$. The beam axial velocity is $\beta_z = 0.1$. The cylindrical ridged cavity parameters are $\theta_o = \pi/2N$ and $N = 6$.
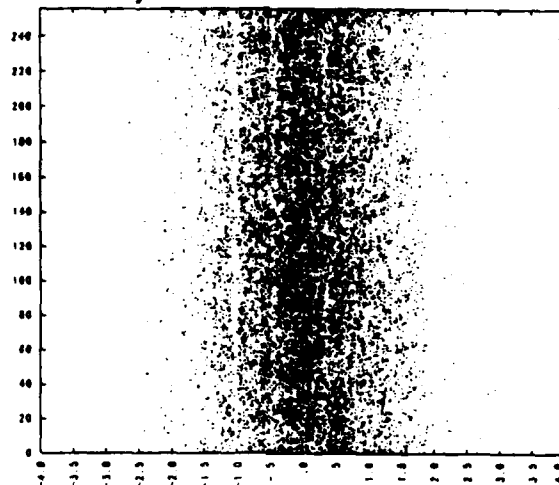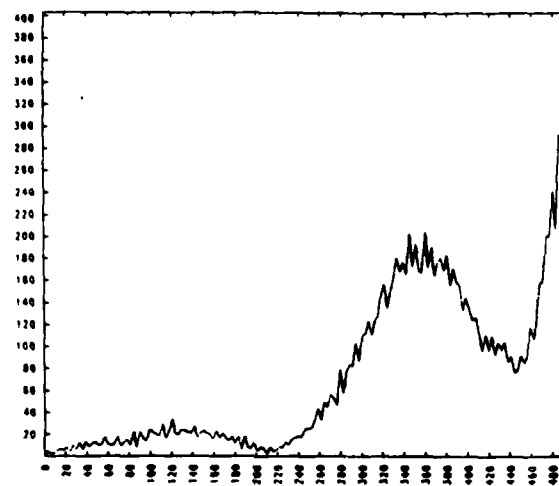
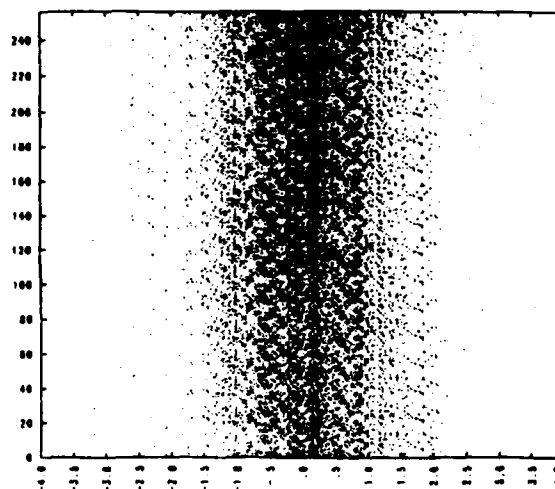ELECTRON PHASE SPACE, T= 300 00

X VERSUS VX

Fig. 1a
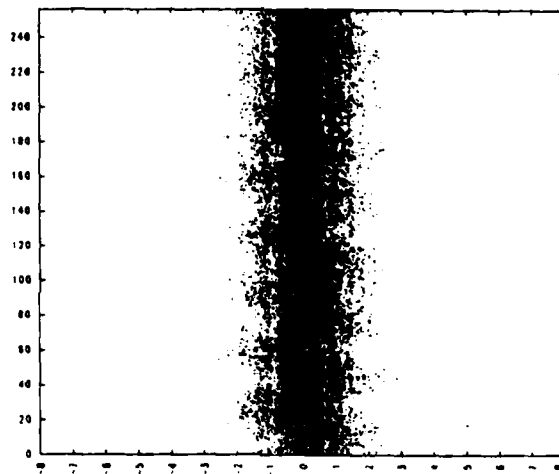
ELECTRON PHASE SPACE, T= 450 00
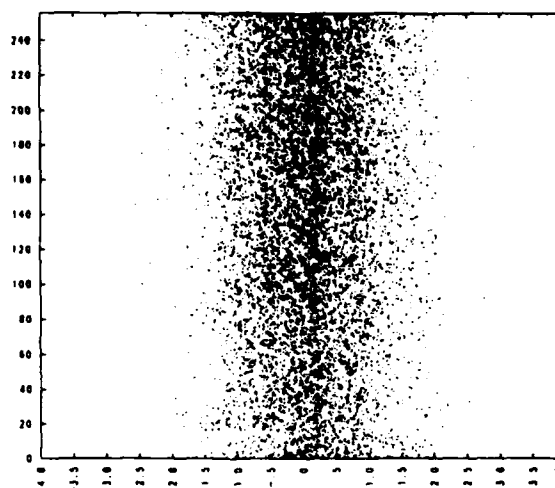
X VERSUS VX

Fig. 1b

EF ENRGY VERSUS   TIME
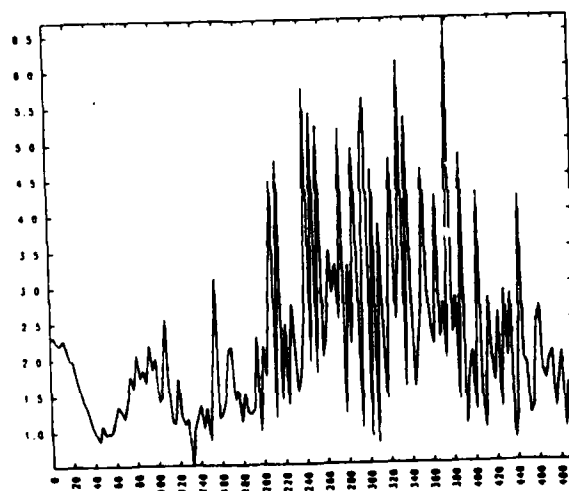
Fig. 1c

16

ELECTRON PHASE SPACE. T= 0.00

X VERSUS VX

Fig. 2a

ELECTRON PHASE SPACE. T= 450.00
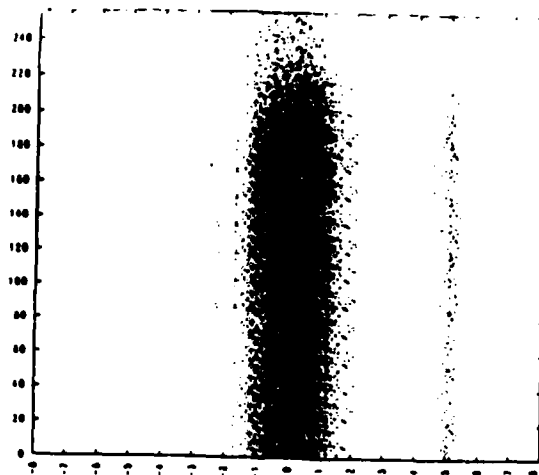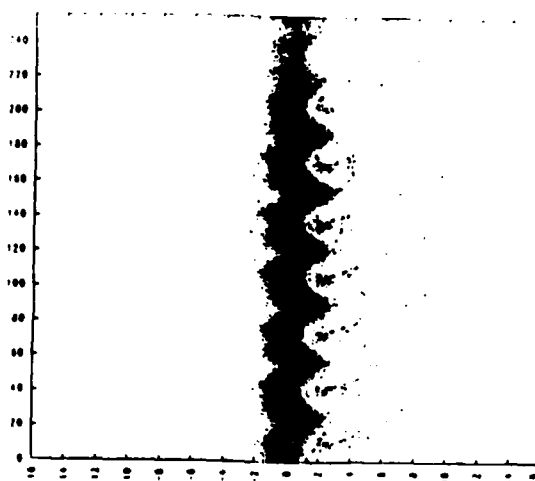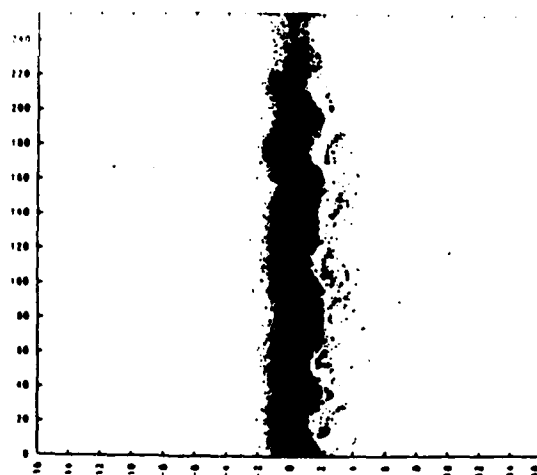
X VERSUS VX

Fig. 2b

EF. ENRGY VERSUS TIME

Fig. 2c

17

ELECTRON PHASE SPACE. T= 0 00

X VERSUS VX

Fig. 3a

ELECTRON PHASE SPACE. T= 50 00

X VERSUS VX

Fig. 3b
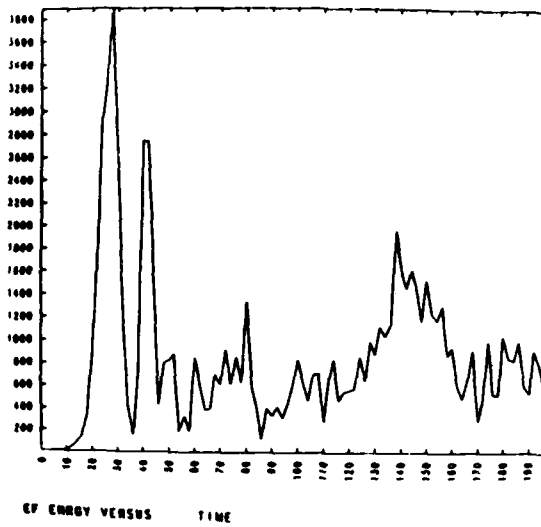
ELECTRON PHASE SPACE. T= 100 00

X VERSUS VX

Fig. 3c

18

EF ENRGY VERSUS   TIME
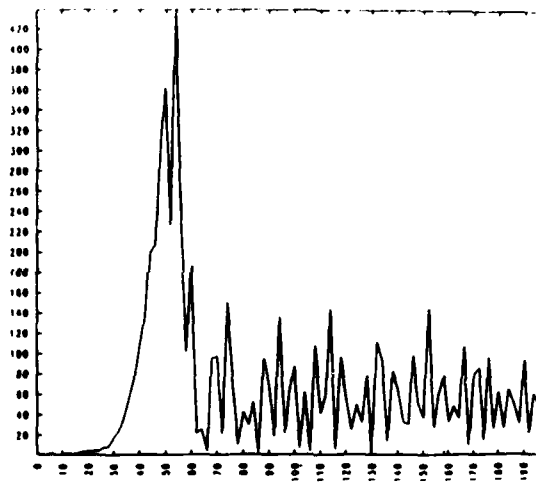
Fig. 4a

EF ENRGY VERSUS   TIME
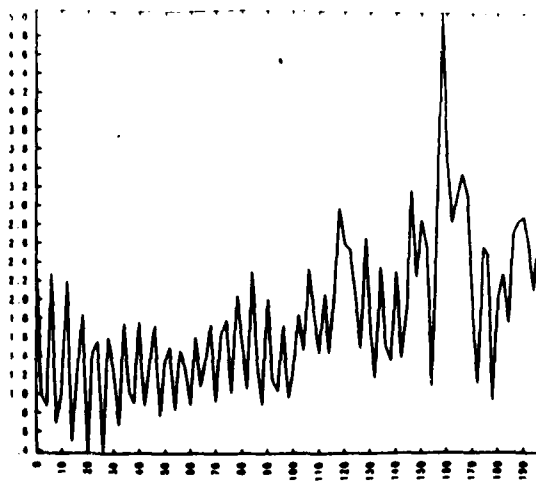
Fig. 4b

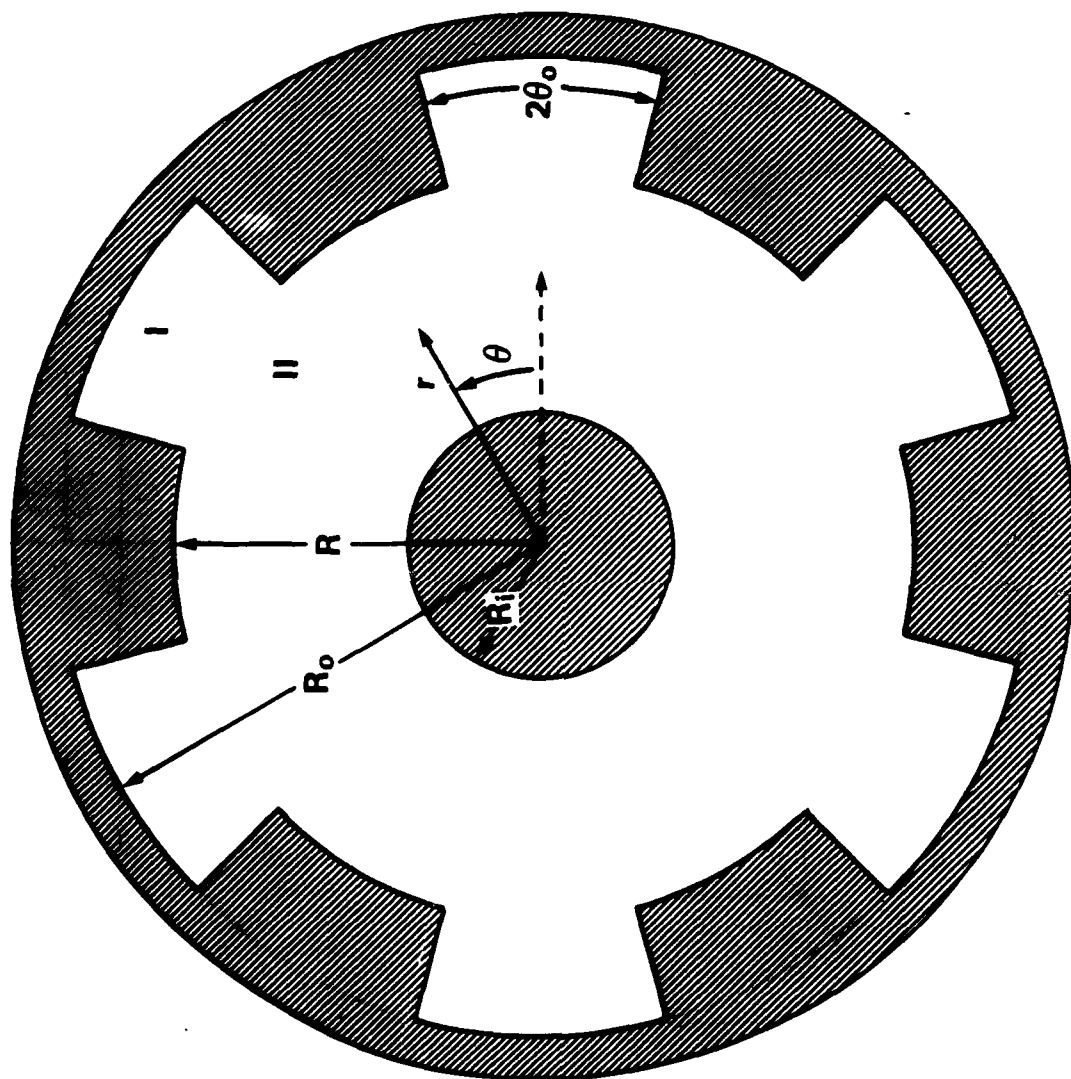EF ENRGY VERSUS   TIME

Fig. 4c
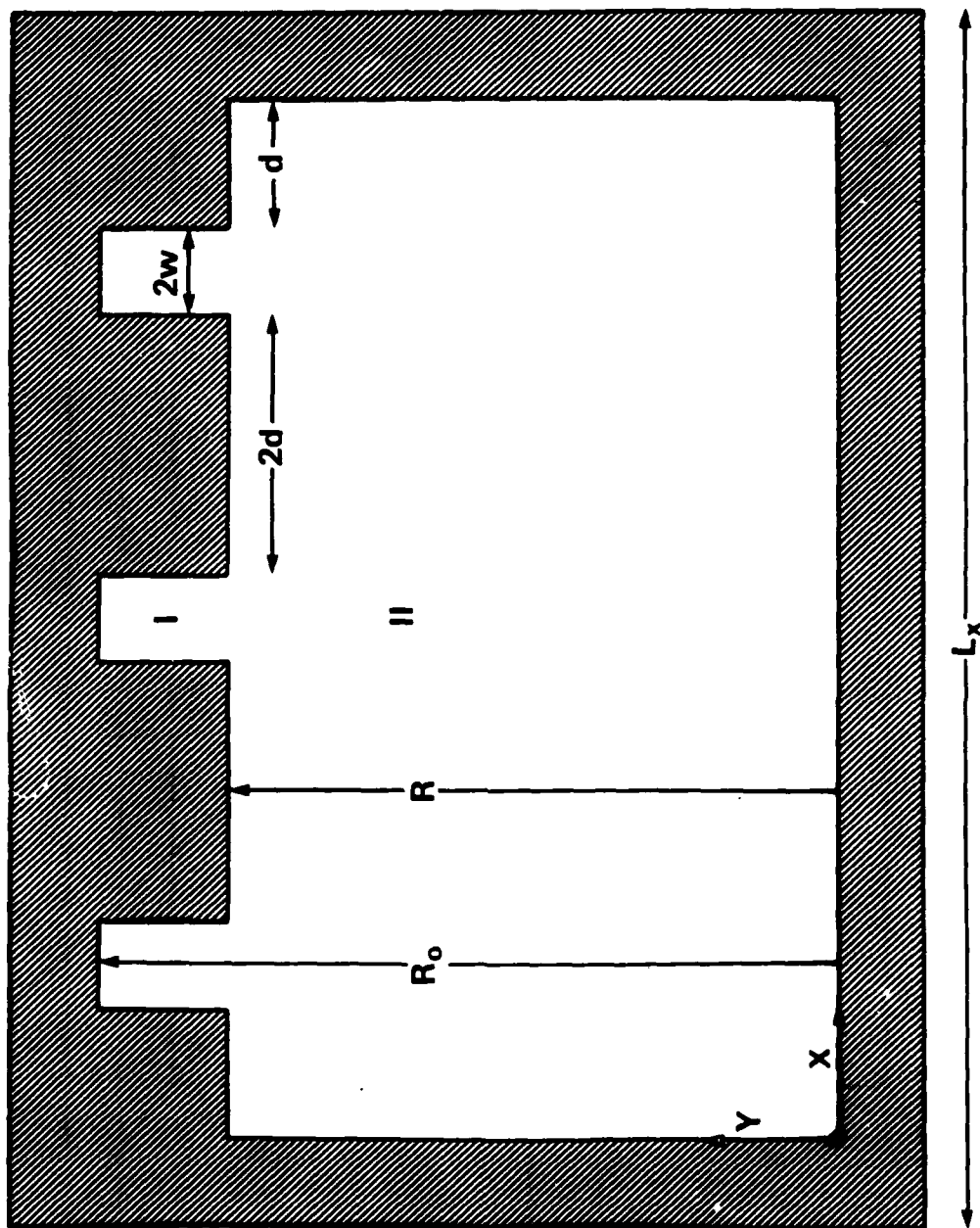
19

Fig. 5a

Fig. 5b

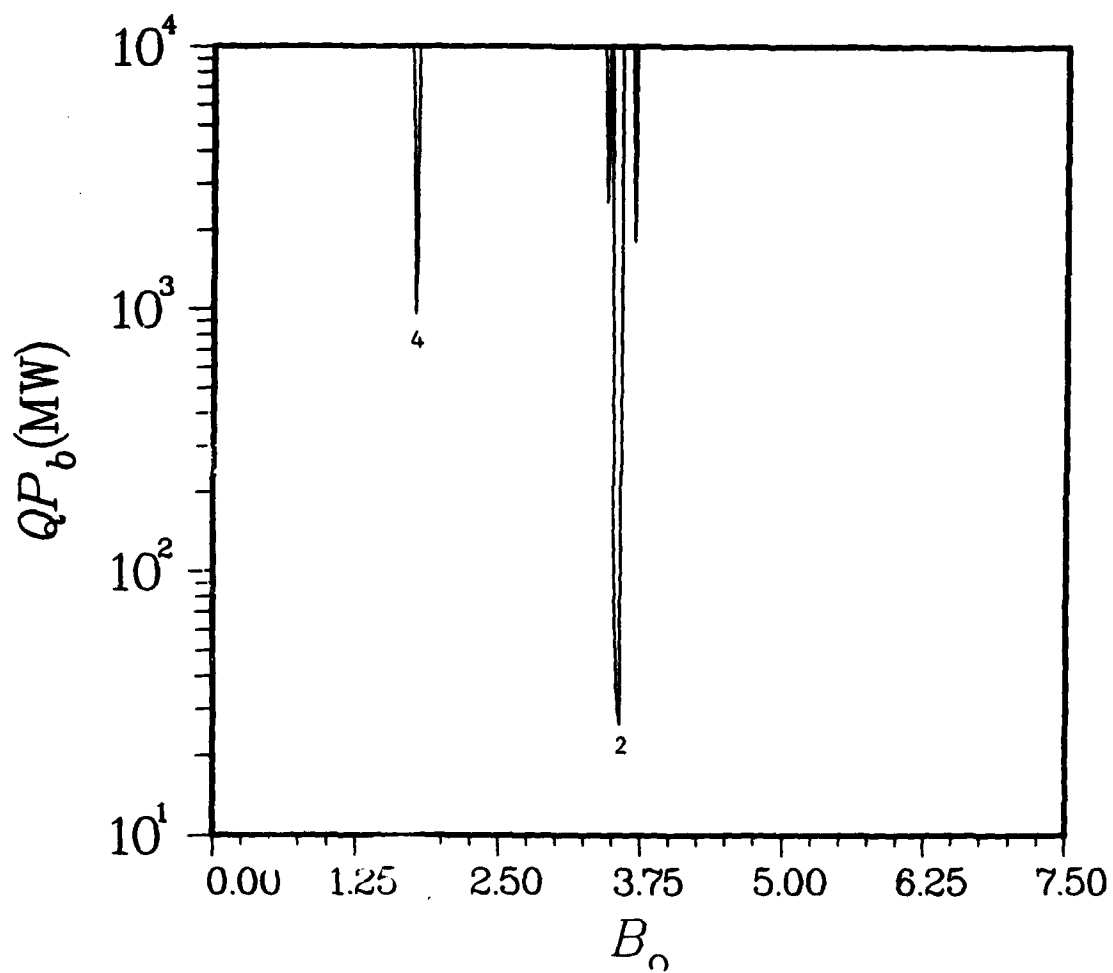# Start Oscillation Beam Power

Fig. 6

22

TE_{021}

$E_{max} = 4.052$

$k_\perp = 5.522$

$L_x = 2.186$

$R_o = 1.198$

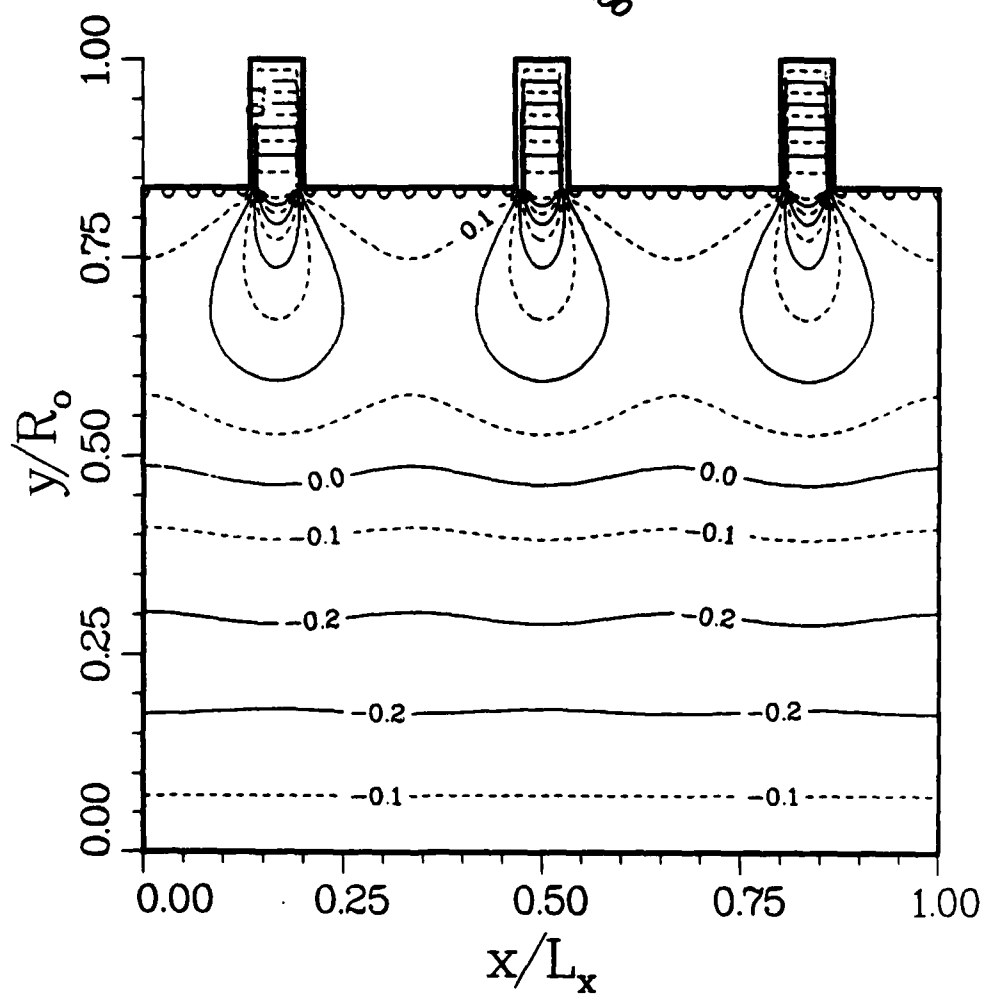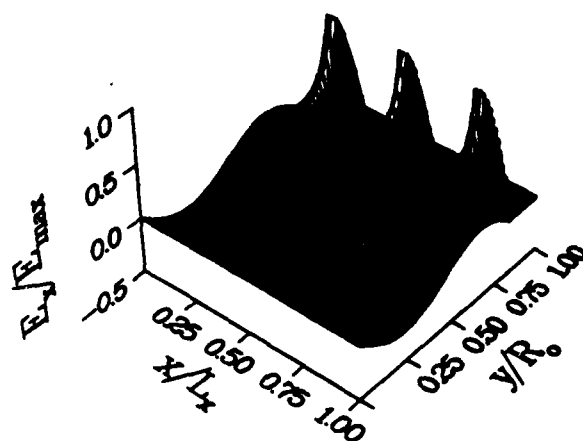$w = 0.055$

Fig. 7

23

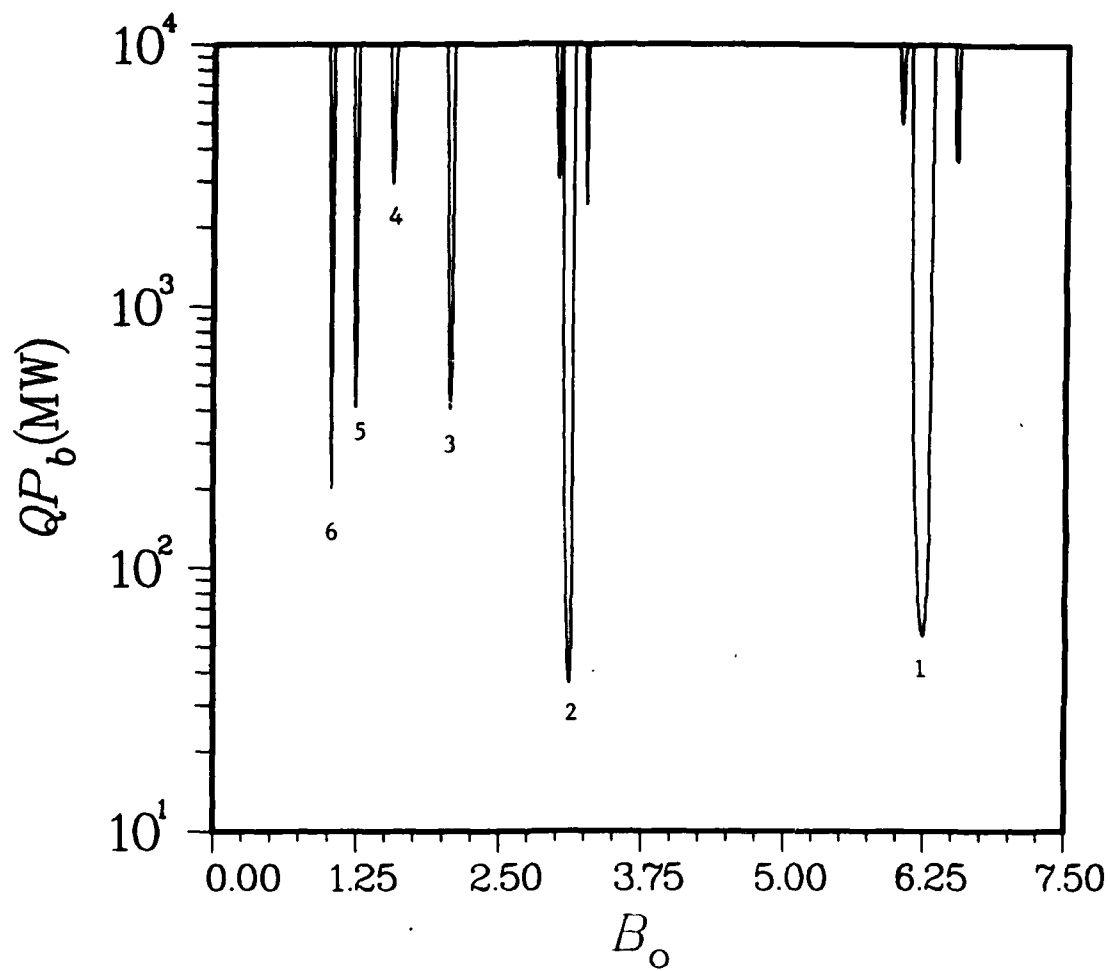# Start Oscillation Beam Power

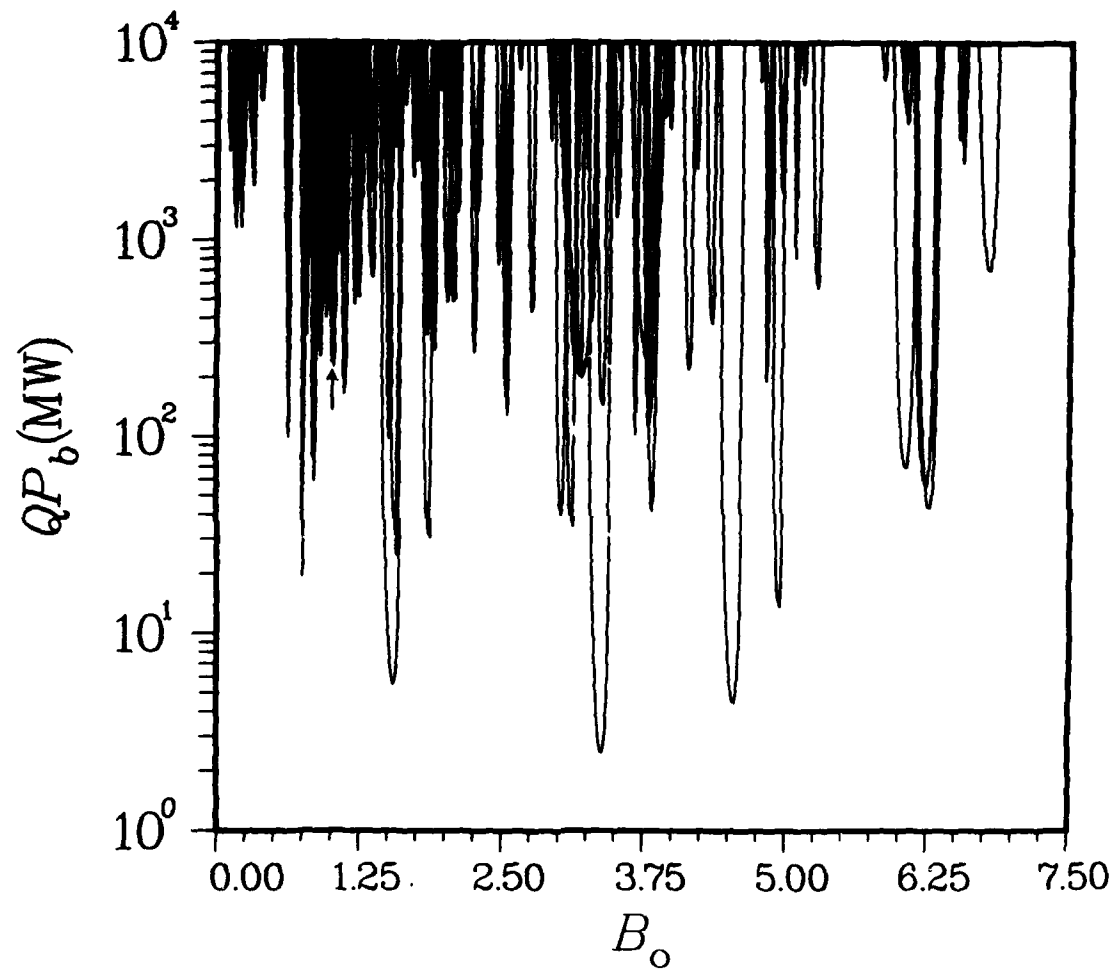Fig. 8

Start Oscillation Beam Power
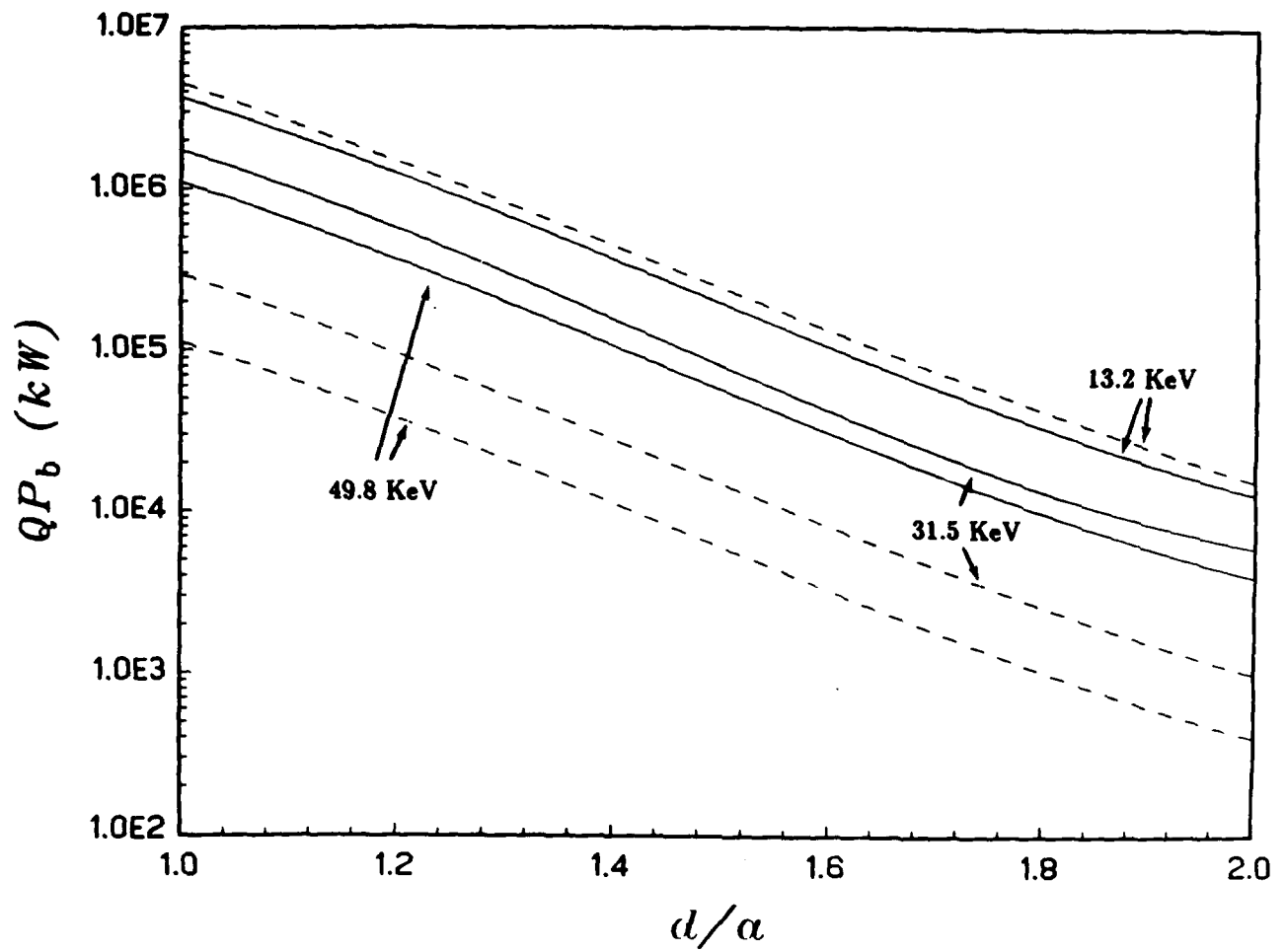

Fig. 9

Start Oscillation

Fig. 10

V. APPENDICES

GYRO-PENIOTRON EMISSION IN A MAGNETRON-TYPE CAVITY*

P. VITELLO

SCIENCE APPLICATIONS INTERNATIONAL CORPORATION
McLEAN, VA 22102 USA

ABSTRACT

We present here a new linear theory formulation of the average energy loss via the electron cyclotron maser and peniotron interactions in a slotted magnetron-type cavity. Use is made of the linear theory results to study start oscillation conditions and mode competition for the high-harmonic gyro-peniotron oscillator. For a magnetron-type cavity, the gyro-peniotron is found to have the same sensitivity to guiding center spread as for a smooth walled cavity. Mode competition, as well as the start oscillation beam power can be reduced however in a slotted cavity geometry. In the non-linear regime, the saturated emission efficiency for a magnetron-type cavity gyro-peniotron is predicted to be as large as has been calculated for a smooth walled cavity device.

INTRODUCTION

The gyro-peniotron oscillator is a device with the potential for extremely high saturated efficiencies for RF emission. Theoretical modeling[1-9] suggests that efficiencies (perhaps as great as 80-90%) can be obtained for electron beams with finite velocity and guiding center spread. Even though the peniotron interaction may lead to higher saturated efficiencies than the electron cyclotron interaction, in the weak field linear limit the cyclotron maser interaction is generally very much stronger. The relative weakness of the peniotron interaction can lead to mode competition and interference from cyclotron maser modes with lower start oscillation beam powers. Use of a slotted, magnetron-type cavity presents a means of both lowering the gyro-peniotron start oscillation current, and at the same time reducing mode competition[8]. We give here a new formulation of the magnetron-type cavity linear theory average beam energy loss (c.f. Reference [10]), and discuss mode competition, start oscillation conditions, and the behavior of the non-linear saturated emission efficiency in such a system.

We will consider a magnetron-type cavity with N slots each of width $2\theta_o$. The cavity inner radius, outer radius, and axial length are respectively a and b, and L. For such a system, the beam averaged change in energy $\delta\bar\gamma$ for an axis symmetric beam of guiding center r_c is given, in the linear regime, by

$$\delta\bar\gamma = \frac{E_o^2}{\gamma_o\left(k_\|\beta_{\|o}\right)^2}\sum_{j=-\infty}^{\infty}\sum_{s=-\infty}^{\infty}a_\Gamma^2 J_{\Gamma-s}^2(\kappa_c)\left\{-\frac{\beta_{\perp o}^2 J_s'^2(\kappa_L)}{\beta_{\|o}}\left(\frac{\omega g'(x)}{k_\|}-\frac{k_\|}{\omega}\frac{\mathrm{d}x^2 g(x)}{\mathrm{d}x}\right)\right.$$

$$+2sJ_s'(\kappa_L)\left(\frac{sJ_s(\kappa_L)}{\kappa_L}\frac{s\Omega}{\omega}-\frac{k_\perp\beta_{\perp o}}{\omega}J_s(\kappa_L)\right)g(x)$$

$$\left.+\frac{k_\perp^2\beta_{\perp o}^2}{2\Omega\omega}\left(J_{s+1}'^2(\kappa_L)g(x^+)-J_{s-1}'^2(\kappa_L)g(x^-)\right)\right\}, \tag{1}$$

28

where $\kappa_c = k_\perp r_c$, $\kappa_L = k_\perp r_L$, $k_\perp$ is the perpendicular wavenumber, r_L is the Larmor radius, $\Gamma = m + jN$, m is an integer which determines the mode, $k_\parallel = l\pi/L$, ω is the cavity frequency, E_o is the RF field amplitude,

$$x = \left(\frac{s\Omega - \omega}{k_\parallel \beta_{\parallel o}}\right), \qquad x^\pm = \left(\frac{(s \pm 1)\Omega - \omega}{k_\parallel \beta_{\parallel o}}\right), \tag{2}$$

$$g(y) = \left(\frac{\cos\left(\pi y/2 + (l-1)\pi/2\right)}{(y^2 - 1)}\right)^2, \tag{3}$$

and

$$a_\Gamma = \frac{\sin\Gamma\theta_o}{\Gamma J_\Gamma'(k_\perp a)}. \tag{4}$$

Dimensionless units with a as the unit of length, a/c as the unit of time, and $m_e c^2/|e|a$ as the unit of electric and magnetic fields are used. Each term in j in above relation for $\delta\bar{\gamma}$ is exactly a_Γ^2 times the value found for the change in energy for a smooth walled cavity with the single mode TE$_{\Gamma nl}$.[11] Electron cyclotron maser emission at the sth cyclotron harmonic comes from the terms containing $g'(x)$ and $dx^2 g(x)/dx$. Electron cyclotron absorption at the sth harmonic comes from the terms in $g(x)$. Peniotron emission at the $(s-1)$th harmonic and absorption at the $(s+1)$th harmonic come respectively from the terms in $g(x^+)$ and $g(x^-)$. For fixed j and s, the relative strengths of each of these interactions are the same as in the smooth cavity case.

If the beam is exactly centered on axis, only the harmonics $s = \Gamma$ contribute to $\delta\bar{\gamma}$. Electron cyclotron emission occurs then at the Γth harmonics, while peniotron emission occurs at the $(\Gamma - 1)$th harmonics. For $N \geq 2$ there is no interference between the two interactions of a fixed m mode. The electron cyclotron maser interaction and peniotron absorption may interfere with peniotron emission if there is a finite spread in guiding centers. As the relative strengths of the interactions are the same as in the smooth cavity case, the limits on guiding center spread are also the same (see Reference [11]). Even with zero guiding center spread, mode competition may take place between peniotron emission from the desired operating m mode and electron cyclotron maser emission from different m modes. Such mode competition can be a serious problem for the high-harmonic smooth walled gyro-peniotron.[5] A N slotted magnetron-type cavity cavity has an imposed Nth fold symmetry, however, which is lacking in a smooth walled cavity. Operating at the high-harmonic $m = \Gamma = s = N/2$ optimizes the amplitude a_Γ, leading to a very strong beam to cavity coupling. For m modes that do not "fit" well into the cavity symmetry, a_Γ is quite small and the beam to cavity coupling is weaker. The overall effect is a reduction in mode competition between the $m = N/2$ mode and other m modes. Besides this reduction in mode competition, a slotted cavity can also have the desirable effect of moving the RF field radial peak inward towards the beam. This produces a stronger interaction, decreasing the start oscillation current, which is relatively high for the smooth walled gyro-peniotron.[10]

In the non-linear limit, as in the linear regime, neighboring s harmonics, differ by at least by N for a beam with small guiding center spread about the axis. If N is large and is one operates at the mode $m = N/2$, only the $s = N/2$ harmonic will show a strong coupling between the beam and the cavity. The other harmonics are weaker due to having either much smaller amplitudes a_Γ or due to the beam particles experiencing

very large phase drifts relative to the RF field during their passage through the cavity. Since only one harmonic would therefore be involved in gyro-peniotron magnetron-type cavity interaction, we expect the same extremely high saturation efficiencies to be obtainable as have been calculated for smooth cavity systems.[3]

CONCLUSION

We show from a linear theory analysis of a slotted magnetron-type cavity oscillator that for each sth harmonic of the cyclotron frequency, the relative relative strength of the electron cyclotron maser interaction and the peniotron interaction terms are the same as for a smooth walled cavity. This leads to a gyro-peniotron with a magnetron-type cavity having the same sensitivity to guiding center spread as is found for a smooth walled system. The optimized saturated emission efficiency for the slotted cavity is predicted to be also as high as has been calculated for the smooth walled gyro-peniotron. A slotted cavity design is likely to be preferable, however, as the imposed symmetry can lead to a reduction in mode competition, and to a decrease in the start oscillation beam current.

REFERENCES

[1] G. Döhler, D. Gallapher, and R. Moats, "The peniotron: A fast wave device for efficient high power mm wave generation," in *Tech. Dig. Int. Electron Devices Meet.*, pp. 400–403, 1978.

[2] S. P. Kuznetsov, D. I. Trubetskov, and A. P. Chetverikov, "Nonlinear analytic theory of the peniotron," *Sov. Tech. Phys. Lett.*, vol. 6, pp. 498–499, 1980.

[3] P. Vitello, "Cyclotron maser and peniotron-like instabilities in a whispering gallery mode gyrotron," *IEEE Trans. Microwave Theory Tech.*, vol. MTT-32, pp. 917–921, 1984.

[4] S. Ono, K. Tsutaki, and T. Kageyama, "Proposal of a high efficiency tube for high power millimeter or submillimeter wave generation: The gyro-peniotron," *Int. J. Electron.*, vol. 56, pp. 507–520, 1984.

[5] P. Vitello, "High harmonic gyro-peniotron oscillator," in *9th Int. Conf. Infrared Millimeter Waves*, (Takarazuka, Japan), Paper T-7-5, 1984.

[6] U. A. Shrivastava and R. W. Grow, "Gyrotron and peniotron modes in rotating-beam devices," in *Int. J. Electron.*, vol. 57, pp. 1077–1096, 1984.

[7] P. Vitello and K. Ko, "The high power gyro-peniotron oscillator," in *10th Int. Conf. Infrared Millimeter, Waves*, (Florida), Paper TH4.2, 1985.

[8] P. S. Rha, L. R. Barnett, J. M. Baird, and R. W. Grow, in Int. Electron Device Meet., pp. 525–538, 1985.

[9] P. Vitello, in preparation.

[10] K. R. Chu and D. Dialetis, "Kinetic theory of harmonic gyrotron oscillator with slotted resonant structure," *Infrared Millimeter Waves*, vol. 13, 45, 1985.

[11] P. Vitello and K. Ko, "Mode competition in the gyro-peniotron," *IEEE Trans. Plasma Sci.*, vol. PS-13, 454, 1985.

Theory of Slotted High Harmonic Gyrotron Oscillators

P. VITELLO

Science Applications International Corporation, McLean, Virginia 22102

and

C. MENYUK

*Science Applications International Corporation, McLean, Virginia 22102, and
Department of Electrical Engineering, University of Maryland Catonsville, MD 21228
and College Park, MD 20742*

Start oscillation conditions are considered for slotted rectangular gyrotron cavities. The energy loss of the electron beam to the cavity RF field is presented in a form where the geometric and the gyrotron instability terms at each harmonic have been separated. It is found that the addition of slots to a cavity lowers the required beam power for the start oscillation condition and can lead to a *decrease* of the start oscillation beam power as the harmonic number is increased. Previous gyrotron cavity designs have consistently shown the start oscillation beam power increasing with harmonic number. These slotted devices thus appear potentially attractive as a means of achieving millimeter wave emission for use in RF heating and plasma diagnostics.

31

Emission in a gyrotron occurs at the harmonics of the electron cyclotron frequency. Promising applications for high power, high frequency gyrotrons include plasma heating, advanced accelerators, and spectroscopy. As the frequency increases, however, either large magnetic fields must be used or operation at high cyclotron harmonics is required. Presently, most gyrotron development has focused on devices using the first or second harmonic.[1-3] These low harmonics necessitate either the use of a superconducting magnet or a pulsed magnetic field if millimeter and sub-millimeter wave frequencies are to be achieved.

High harmonic gyrotron emission has been demonstrated for several tube designs. Using smooth-walled, cylindrical cavities with an axis encircling beam, harmonics as high as $m = 11$ have been observed for a TE_{m1l} "whispering gallery" mode gyrotron oscillator.[4-5] High energy, large Larmor orbit beams are required for "whispering gallery" mode gyrotrons as the modes are concentrated towards the wall of the cavity. Also with an axis encircling beam with high energy (2 MeV) electrons, strong emission at the 12th harmonic has been generated using a slotted cylindrical tube.[6] Further investigations of slotted rectangular and ridged rectangular tubes[7-9] and of slotted cylindrical tubes[10-18] has shown that even for moderate beam energies, strong high harmonic fringe fields can be positioned at the beam orbits. All of these studies show that slotted structures greatly increase the high harmonic interaction in a gyrotron.

While high harmonic gyrotron oscillators and gyro-TWT amplifiers have been studied for cylindrical slotted tubes, only gyro-TWT amplifiers have been been investigated in any detail for rectangular slotted systems. In this letter, we study high harmonic emission in rectangular, slotted gyrotron oscillators. We find that the addition of slots to a rectangular gyrotron cavity greatly enhances the interaction between the electron beam and the cavity RF field at high harmonics. This enhancement is so great that, under some circumstances, the interaction strength can actually *increase*

32

with harmonic number. As a consequence, these devices are a potentially interesting source of millimeter wave radiation.

The slotted rectangular cavity considered is shown in Figure 1. We will use N to designate the number of slots and L_z the axial length of the cavity. The inner and outer slot y dimensions are R and R_o, while the cavity width in the x direction is given as L_x. The distance $2d$ between the slots equals twice the distance from the first or last slot to the tube wall, while the slot width is $2w$. We expect that qualitatively our results would apply to other slotted or ridged rectangular cavity designs which show strong fringe fields, such as that used for the peniotron.[19-20] In the following we make use of dimensionless units, with the cavity transverse length R being our scaling parameter. In these units, length is measured in units of R, frequency in units of c/R, and the background magnetic and RF fields are measured in units of $m_e c^2/|e|R$, where m_e is the electron rest mass, e is the electron charge, and c is the speed of light. The dimensionless cyclotron frequency Ω/γ is equal in these units to B_o/γ where B_o is the assumed constant background axial magnetic field and γ is the Lorentz factor.

To determine the RF fields, it it convenient to expand the RF field separately in the cavity proper (Region I) and in the slots (Region II) in terms of the local regional eigenfunctions, and to then match the fields across the slot openings. We take the relative phase dependence of each of the N slots as being $\cos[\pi(q+1/2)m/N]$, where $q = 0, \ldots, N-1$ is the slot number. The value of the mode number m determines the overall mode. The 2π mode corresponds to $m = 0$, while the π mode is given by $m = N$. In order to obtain a closed analytic form for the field solution, an infinite sum over Γ, where $k_z = \Gamma\pi/L_z$, is used only in Region I, with just a single term, $k_z = 0$, being kept in Region II. This approximation is described in Ref. 7. Only the non-negative terms which satisfy $\Gamma = 2Nj \pm m$, and $j = 0, 1, 2, \ldots$ are allowed. The cavity frequency, $w = (k_\perp^2 + k_z^2)^{1/2}$, for the lth axial mode ($k_z = l\pi/L_z$) is determined

from the cavity mode m by solving the dispersion relation

$$\frac{2Nw}{L_z}\sum_{\Gamma}\frac{k_{\perp}}{1+\delta_{\Gamma 0}}\left[\frac{\sin(k_{z_{\Gamma}}w)}{k_{z_{\Gamma}}w}\right]^2\frac{\cot(k_{y_{\Gamma}})}{k_{y_{\Gamma}}}=\cot\left[k_{\perp}(1-R_o)\right],\qquad(1)$$

where $k_{y_{\Gamma}}=(k_{\perp}^2-k_{z_{\Gamma}}^2)^{1/2}$.

To solve for the interaction of the beam with the TE RF cavity field and a constant axial magnetic field we have used the linearized relativistic single particle equation of motion, $d\vec{U}/dz=-(\gamma/U_z)\left[\vec{E}+(\vec{U}\times\vec{B}/\gamma)\right]$ in the guiding center coordinates $(x_{gc},\ y_{gc})$, where $\vec{U}=\gamma\vec{\beta}$ is the product of the electron velocity $\vec{\beta}$ and the Lorentz factor. After averaging over initial time t_o and phase angle φ_o of the beam, the change in the beam energy after passing through the oscillator cavity $\langle\delta\gamma\rangle_{t_o,\varphi_o}$ can be calculated using the standard techniques of linear theory.[7, 21] The details will be presented elsewhere. We find that $\langle\delta\gamma\rangle_{t_o,\varphi_o}$ can be expressed in the compact form

$$\langle\delta\gamma\rangle_{t_o,\varphi_o}=\sum_{s=-\infty}^{\infty}\left|\sum_{\Gamma}\mathcal{A}_{\Gamma}\mathcal{D}_{\Gamma s}\right|^2\left[\text{Re}\left(\mathcal{F}_s\right)+i\text{Im}\left(\mathcal{F}_s\right)\right],\qquad(2)$$

where $\mathcal{A}_{\Gamma}$ is the Γth amplitude of the RF field in Region I, $\mathcal{D}_{\Gamma s}$ is the s harmonic contribution to the guiding center expansion of the Γth RF field term, and $\mathcal{F}_s$ gives the s harmonic gyrotron interaction terms. Again, only the non-negative terms which satisfy $\Gamma=2Nj\pm m$, where $j=0,1,2,\dots$ are allowed in equation (2).

The full behavior of $\langle\delta\gamma\rangle_{t_o,\varphi_o}$ is given by equation (2). The guiding center dependence is contained entirely in the factor $\left|\sum_{\Gamma}\mathcal{A}_{\Gamma}\mathcal{D}_{\Gamma s}\right|^2$, which is sensitive to the fringe fields generated by the slots, while the resonance behavior as a function of magnetic field about the cyclotron harmonics is given by $\mathcal{F}_s$ which contains the cyclotron maser, Weibel, and peniotron resonances. The contributions from $\text{Re}(\mathcal{F}_s)$ and $\text{Im}(\mathcal{F}_s)$ respectively determine the gyrotron start oscillation beam power and resonant frequency detuning.

Equation (2) can be simplified if a ribbon beam parallel to the x axis is used. Averaging over the x_{gc} guiding center position leads to a reduction of the double sum

34

over cavity eigenfunctions inherent in $|\sum_\Gamma A_\Gamma \mathcal{D}_{\Gamma s}|^2 = \sum_\Gamma A_\Gamma^* \mathcal{D}_{\Gamma s}^* \sum_\Lambda A_\Lambda \mathcal{D}_{\Lambda s}$, to a single sum if the ribbon beam is uniformly distributed at a fixed y_{gc}. After averaging the product $\sum_\Gamma A_\Gamma^* \mathcal{D}_{\Gamma s}^* \sum_\Lambda A_\Lambda \mathcal{D}_{\Lambda s}$ can be replaced by a factor of the form $\sum_\Gamma A_\Gamma^2 \overline{\mathcal{D}}_{\Gamma s}$. Realistically, however, the averaging can not be taken from $x_{gc} = 0$ to $x_{gc} = L_x$ as the beam can not be placed closer to the cavity wall than its Larmor radius. If $m = 2Ni$, where $i = 0, 1, \ldots$ then there is a N-fold periodicity in x for the RF field and the simplifying guiding center averaging can equivalently be taken over any of the regions from $x_{gc} = L_x(j/N)$ to $x_{gc} = L_x(k/N)$, where $0 < j < N - 1$, and $j < k < N$. This also implies that the guiding center averaged energy loss $\langle \delta\gamma \rangle_{t_o, \varphi_o, x_{go}}$ would be unaffected by the extension of the cavity in the x direction to include addition slotted regions.

The cavity geometry determines $k_\perp$ and the magnitude of each s harmonic contribution to the overall RF cavity field of a particular mode. For each s harmonic, $\mathcal{F}_s$ varies with the cavity geometry only through changes in $k_\perp$. Since the addition of slots may generate strong fringe fields without a significant change in $k_\perp$, the predominant change at high harmonic to $\langle \delta\gamma \rangle_{t_o, \varphi_o}$ generally comes from the factor $|\sum_\Gamma A_\Gamma \mathcal{D}_{\Gamma s}|^2$.

The start oscillation beam power and the frequency detuning equation for steady state operation for any TE mode can be found directly from $\langle \delta\gamma \rangle_{t_o, \varphi_o}$. Taking the unperturbed beam energy to be P_b, the total net energy transferred from the beam to the cavity fields is given by $P_b \langle \delta\gamma \rangle_{t_o, \varphi_o} / (\gamma_o - 1)$.[22] Quite generally, the starting power can be given by

$$QP_b = -8.6 \times 10^6 \mathcal{W}(\gamma_o - 1) / Re(\langle \delta\gamma \rangle_{t_o, \varphi_o}) \text{ kW}, \tag{3}$$

and the frequency detuning due to the presence of the beam is

$$\frac{\omega - \omega_o}{\omega_o} = -\frac{1}{2Q} \frac{Im(\langle \delta\gamma \rangle_{t_o, \varphi_o})}{Re(\langle \delta\gamma \rangle_{t_o, \varphi_o})}, \tag{4}$$

where W is the time averaged, volume integrated RF field energy of the cavity, and ω_o is the cold cavity frequency. For gyrotron tubes, the quality factor Q is due mainly to diffractive losses and, with an accurate estimate of its value obtained from cold cavity tests, provides a good approximation of the actual start oscillation power required. By contrast, the linear theory values for the frequency detuning often differ significantly from the detuning under normal high field operating conditions[22] and should used with caution.

We find that the addition of slots can not only enhance enormously the high harmonic interaction and hence greatly lower QP_b, but this enhancement at fixed beam position can *increase* with increasing harmonic number. This rapid decrease in the start oscillation condition with increasing harmonic number has not previously been noted for any gyrotron device. We note that the strongest coupling to our cavity slots occurs for $m = 0$ modes. For these modes the following parameter range was found to result in strong high harmonic interaction with increases with harmonic number: $|\sin k_\perp|^{-1} \simeq 1$ (implies large fringe fields generated by the slots); $L_x \lesssim 2N/n$, where n is the transverse y mode number (all k_{y_r} for $\Gamma \neq 0$ imaginary); and $\sin 2\pi N w / L_x \simeq 1$ (strong beam coupling to the lowest order $\Gamma \neq 0$ fringe field term). We expect proper beam placement in other cavity designs with fringe fields similar to those in a slotted rectangular cavity would also result in enhanced high harmonic coupling with increasing harmonic number.

As an example of how the addition of slots to a rectangular cavity gyrotron oscillator enhances the high harmonic emission we will consider the start oscillation condition QP_b for the cavity and beam parameters investigated by Han and Ferendeci[7] for a slotted rectangular cavity gyro-TWT. For the cavity mode we use $m = 0$, $l = 1$, and the second y transverse mode (*i.e.* the TE_{021} mode), which Han and Ferendeci found to give strong sixth harmonic emission. The cavity parameters are $L_x = 2.186$, $L_z = 15$, $R_o = 1.198$, $w = 0.05466$, and $N = 3$. For the beam parameters we

use a total energy of 70.82 keV, and $\beta_z = 0.268$, which corresponds to $\gamma_o = 1.139$, $U_\perp = 0.45086$, and $U_z = 0.30514$. The electron beam is centered in Region I at $x_{gc} = L_z/2$, $y_{gc} = R/2$. Figure 2 shows the variation of the magnitude of the RF electric field, $|E| = \left(E_z^2 + E_y^2\right)^{1/2} / E_o \sin(k_z z)$, across the cavity opening for these parameters. Shown in the figure are the values for the total field energy per unit length, $\mathcal{W}_T = \mathcal{W}/L_z$, and the field energy per unit length in the slots, $\mathcal{W}_R$. The large fringe field observed in this figure couples very strongly with high harmonic emission. This coupling will be significant at high harmonics since with rising harmonic number s the growth of the the Larmor radius, $r_L \simeq s\beta_\perp/\omega$, allows the beam to increasingly penetrate the fringe fields. In Figure 3 we show QP_b as a function of magnetic field for multiple harmonic emission. Harmonics greater than the sixth are not shown as the beam Larmor radius would be greater that one-half the cavity width R. For comparison, we also show QP_b for a smooth-walled rectangular cavity. For the slotted cavity, harmonics for $s = 1$–3 are dominated by the electron cyclotron maser instability. The fourth harmonic is due to the peniotron instability. For harmonics $s \geq 5$, both the electron cyclotron maser and peniotron instabilities strongly contribute.

As the sensitivity to guiding center is of great importance, we have given in Figures 4a–4d the function $\mathcal{E}^s \equiv |\sum_\Gamma A_\Gamma D_{\Gamma s}| / \mathcal{W}_T^{1/2}$ for $s = 3,4,5,6$. Only the portion of Region I which is at least one Larmor radius from the cavity walls is considered. From equation (3) it is clear that $QP_b \propto (\mathcal{E}^s)^{-2}$. One can see that the interaction at each harmonic rapidly increases near the slot openings due to the fringe fields, and that for $s = 3,4,5$ there are values of y_{gc} for which there is little dependence on x_{gc} of the beam, cavity-coupling. These values would be ideal for the placement of a ribbon beam with an extensive x width. For sixth harmonic operation with a ribbon beam, the cavity design would need to be modified to reduce the rapid variation in QP_b with x_{gc} in the accessible region of the cavity.

For our example, the strong high harmonic coupling which increases with harmonic number was observed even when the beam quality was decreased by assuming a guiding center spread $\delta \bar{x}_{gc} \lesssim 0.2$, $\delta y_{gc} \lesssim 0.1$, and an axial velocity spread $\delta \beta_z \lesssim 0.2\beta_z$. A Gaussian axial velocity distribution was assumed with constant beam energy. The net affect was actually to decrease QP_b as the interaction strength in the linear regime is a rapidly increasing function of both y_{gc} and β_z^{-1}. In general, the magnitude of the beam quality affects will depend upon the details of the gyrotron design.

In conclusion we find that the high harmonic interaction observed here for the slotted rectangular cavity shows great potential for the practical development of a high frequency, low magnetic field gyrotron oscillator. Very high power sources are possible in a wide cavity with multiple slots if a ribbon electron beam is used to reduce space charge limitations. As the basic gyrotron instabilities do not depend upon the cavity geometry, high efficiency emission is expected for the slotted rectangular gyrotron, especially if the system is optimized for emission via the peniotron interaction.[23] Further research into the questions of mode competition and non-linear efficiency needs to be carried out in order to determine how best to take advantage of the slotted cavity fringe field interaction for gyrotron devices.

References

[1] J. M. Baird, in *Tech. Dig. Int. Electron Devices Meet.*, 156 (1979).

[2] R. S. Symons and H. R. Jory, in *Advances in Electronics and Electron Physics*, edited by L. Marton and C. Marton, **55**, 1, (Academic, New York, 1981).

[3] V. L. Granatstein, M. Read, and L. R. Barnett, Int. J. Infrared Millimeter Waves, **5**, 267 (1984).

[4] D. B. McDermott, N. C. Luhmann, Jr., and D. S. Furuno, in *Eighth Int. Conf. Infrared Millimeter Waves*, TH4.1 (1983).

[5] D. B. McDermott and N.C. Luhmann, Jr., Proc. SPIE, **423**, 58 (1983).

[6] W. W. Destler, R. L. Weiler, and C. D. Striffler, Appl. Phys. Lett., **38**, 570 (1981).

[7] A. M. Ferendeci and C. C. Han, Int. J. Infrared Millimeter Waves, **6**, 1267 (1985).

[8] C. C. Han and A. M. Ferendeci, Int. J. Electron., **57**, 1055 (1984).

[9] Q. F. Li and J. L. Hirshfield, Int. J. Infrared Millimeter Waves, **7**, 71 (1986).

[10] Y. Y. Lau and L. R. Barnett, Int. J. Infrared Millimeter Waves, **3**, 619 (1982).

[11] P. S. Rha, L. R. Barnett, J. M. Baird, and R. W. Grow, in *Int. Electron Device Meet.*, 525 (1985).

[12] R. W. Grow and U. A. Shrivastava, in *Int. Electron Devices Meet.*, 384 (1982).

[13] H. S. Uhm, C. M. Kim, and W. Namkung, Phys. Fluids, **27**, 488 (1984).

[14] K. R. Chu and D. Dialetis, Int. J. Infrared Millimeter Waves, **5**, 37 (1984).

[15] K. R. Chu and D. Dialetis, Infrared Millimeter Waves, **13**, 45 (1985).

[16] J. Y. Choe and W. Namkung, IEEE Trans. Nuclear Sci., **NS-32**, 2882 (1985).

[17] U. A. Shrivastava, R. W. Grow, P. S. Rha, J. M. Baird, and L. R. Barnett, Int. J. Electron., **61**, 33 (1986).

[18] P. Vitello, in *Eleventh International Conf. Infrared Millimeter Waves*, Tirrenia, Pisa, Italy, 46 (1986).

[19] S. Ono, K. Tsutaki, and T. Kageyama, in *Int. Electron Devices Meet.*, 456 (1983).

[20]G. Döhler, D. Gallagher, R. Moats, and F. Scafuri in *Int. Electron Devices Meet.*, 328 (1981).

[21]P. Vitello and K. Ko, IEEE Trans. Plasma Sci., PS-13, 454 (1985).

[22]G. F. Brand, Int. J. Infrared Millimeter Waves, 4, 919 (1983).

[23]P. Vitello, Int. J. Infrared Millimeter Waves, 8, 487 (1987).

Figure Captions

FIG. 1. Cross-section of the slotted rectangular gyrotron.

FIG. 2. RF electric field magnitude across the slotted rectangular cavity for the TE_{021} mode. Contours are shown at intervals of 1/15 of the maximum value of $|E|$.

FIG. 3. TE_{021} mode start oscillation condition for the rectangular cavity. The solid curves gives QP_b for the slotted cavity, while the dashed curve gives QP_b for the case without slots. Each emission resonance is labeled by its harmonic number s.

FIG. 4(a). Surface and contour plot for $\mathcal{E}^s$ for $s = 3$. Contours are shown at intervals of 1/15 of the maximum value of $\mathcal{E}^s$.

FIG. 4(b) Surface and contour plot for $\mathcal{E}^s$ for $s = 4$. Contours are shown at intervals of 1/15 of the maximum value of $\mathcal{E}^s$.

FIG. 4(c). Surface and contour plot for $\mathcal{E}^s$ for $s = 5$. Contours are shown at intervals of 1/15 of the maximum value of $\mathcal{E}^s$.

FIG. 4(d). Surface and contour plot for $\mathcal{E}^s$ for $s = 6$. Contours are shown at intervals of 1/15 of the maximum value of $\mathcal{E}^s$.
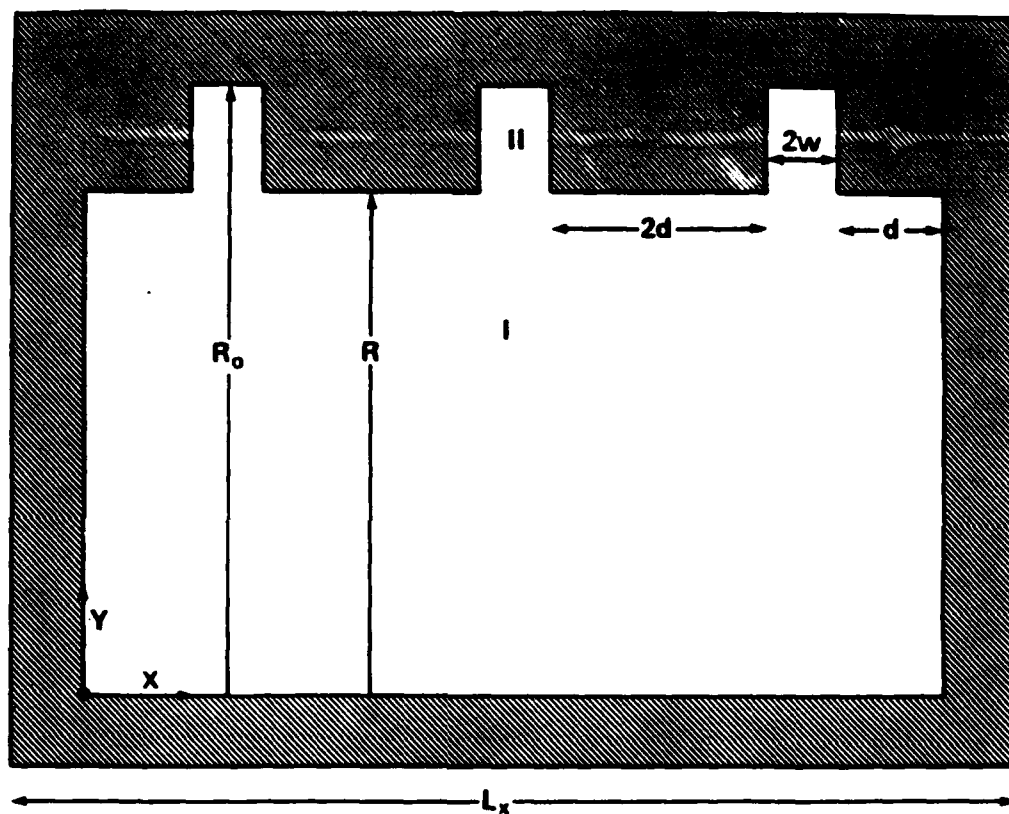
41

FIG. 1. Cross-section of the slotted rectangular gyrotron.

TE_{021}

$|E|_{max} = 4.555*10^{0}$

$k_{\perp} = 5.522$

$L_x = 2.186$

$R_o = 1.198$

$w = 5.466*10^{-2}$
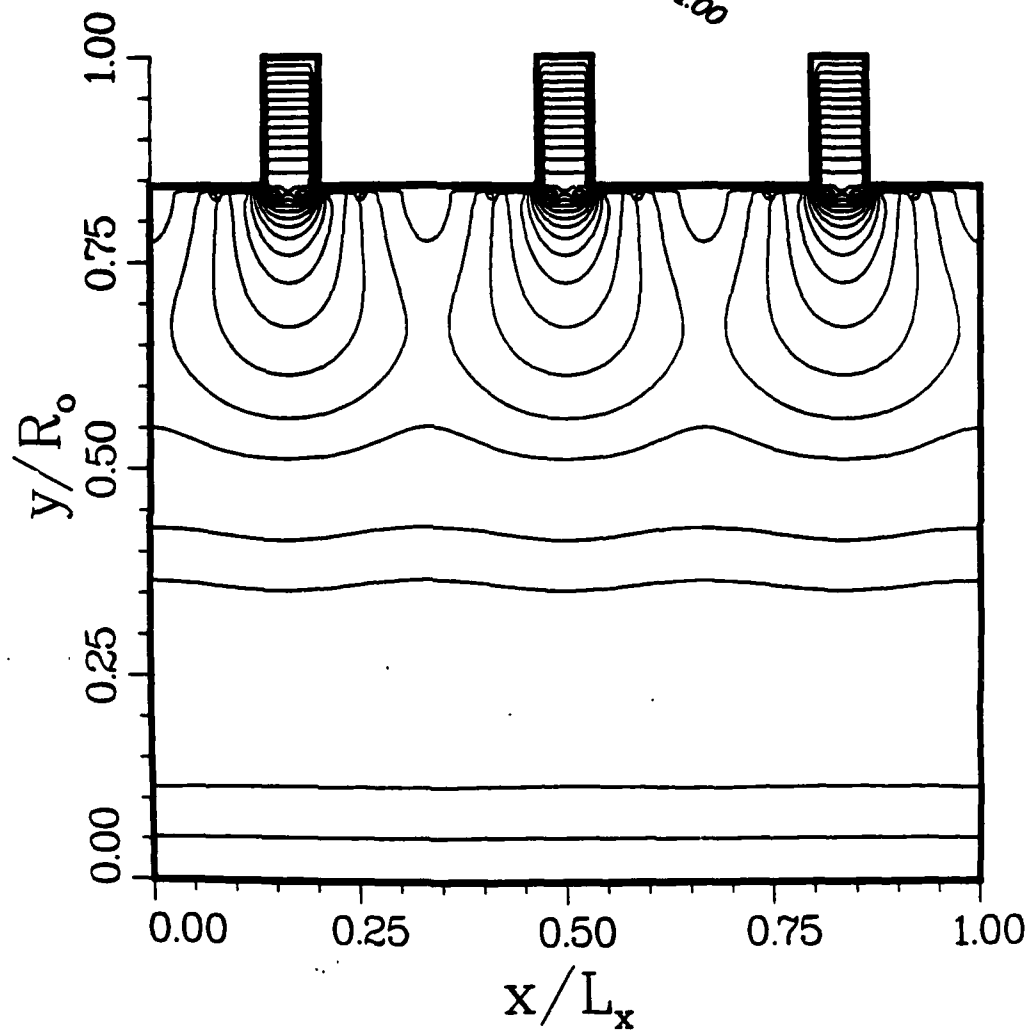
$W_R = 1.325*10^{-2}$

$W_T = 3.498*10^{-2}$

FIG. 2. RF electric field magnitude across the slotted rectangular cavity for the TE_{021} mode. Contours are shown at intervals of 1/15 of the maximum value of $|E|$.
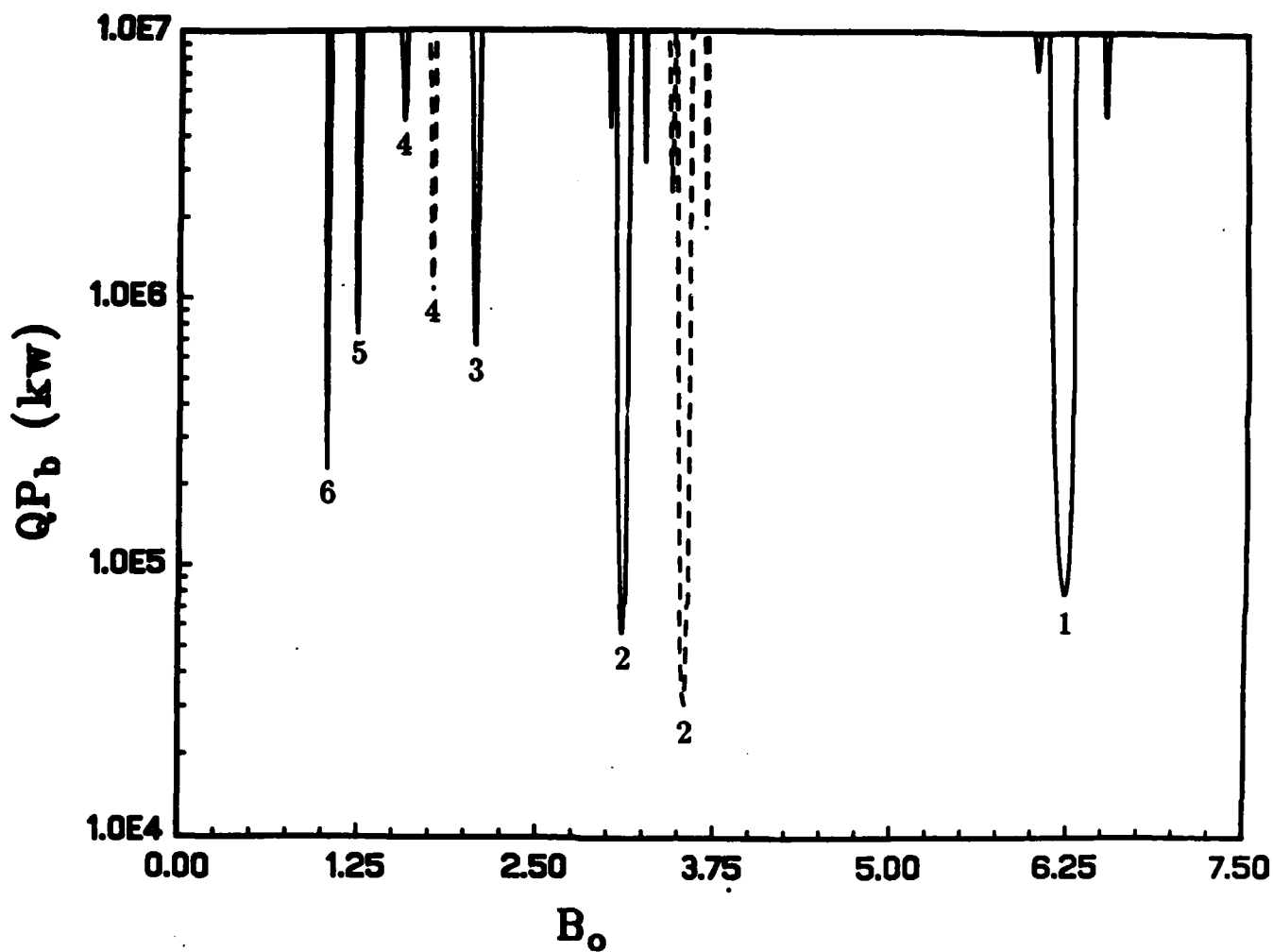
FIG. 3. TE$_{021}$ mode start oscillation condition for the rectangular cavity. The solid curves gives QP_b for the slotted cavity, while the dashed curve gives QP_b for the case without slots. Each emission resonance is labeled by its harmonic number s.

TE_{021}^3

$\mathscr{E}_{min} = 1.597*10^{-1}$

$\mathscr{E}_{max} = 1.597*10^1$

$k_\perp = 5.522$

$L_x = 2.186$

$R_o = 1.198$

$w = 5.466*10^{-2}$

$\mathscr{W}_R = 1.325*10^{-2}$

$\mathscr{W}_T = 3.498*10^{-2}$

FIG. 4(a). Surface and contour plot for $\mathscr{E}^s$ for $s = 3$. Contours are shown at intervals of 1/15 of the maximum value of $\mathscr{E}^s$.

45

TE_{021}^4

$\mathscr{E}_{min} = 1.309*10^{-1}$

$\mathscr{E}_{max} = 3.227*10^1$

$k_\perp = 5.522$

$L_z = 2.186$

$R_o = 1.198$

$w = 5.466*10^{-2}$

$W_R = 1.325*10^{-2}$

$W_T = 3.498*10^{-2}$

FIG. 4(b) Surface and contour plot for $\mathscr{E}^s$ for $s = 4$. Contours are shown at intervals of 1/15 of the maximum value of $\mathscr{E}^s$.

TE_{021}^5

$\mathscr{E}_{min} = 1.868*10^0$

$\mathscr{E}_{max} = 6.532*10^1$

$k_\perp = 5.522$

$L_x = 2.186$

$R_o = 1.198$

$w = 5.466*10^{-2}$

$W_R = 1.325*10^{-2}$

$W_T = 3.498*10^{-2}$

FIG. 4(c). Surface and contour plot for $\mathscr{E}^s$ for $s = 5$. Contours are shown at intervals of 1/15 of the maximum value of $\mathscr{E}^s$.

47

$$TE_{021}^6$$

$\mathcal{E}_{min} = 1.980*10^1$

$\mathcal{E}_{max} = 1.187*10^2$

$k_\perp = 5.522$

$L_z = 2.186$
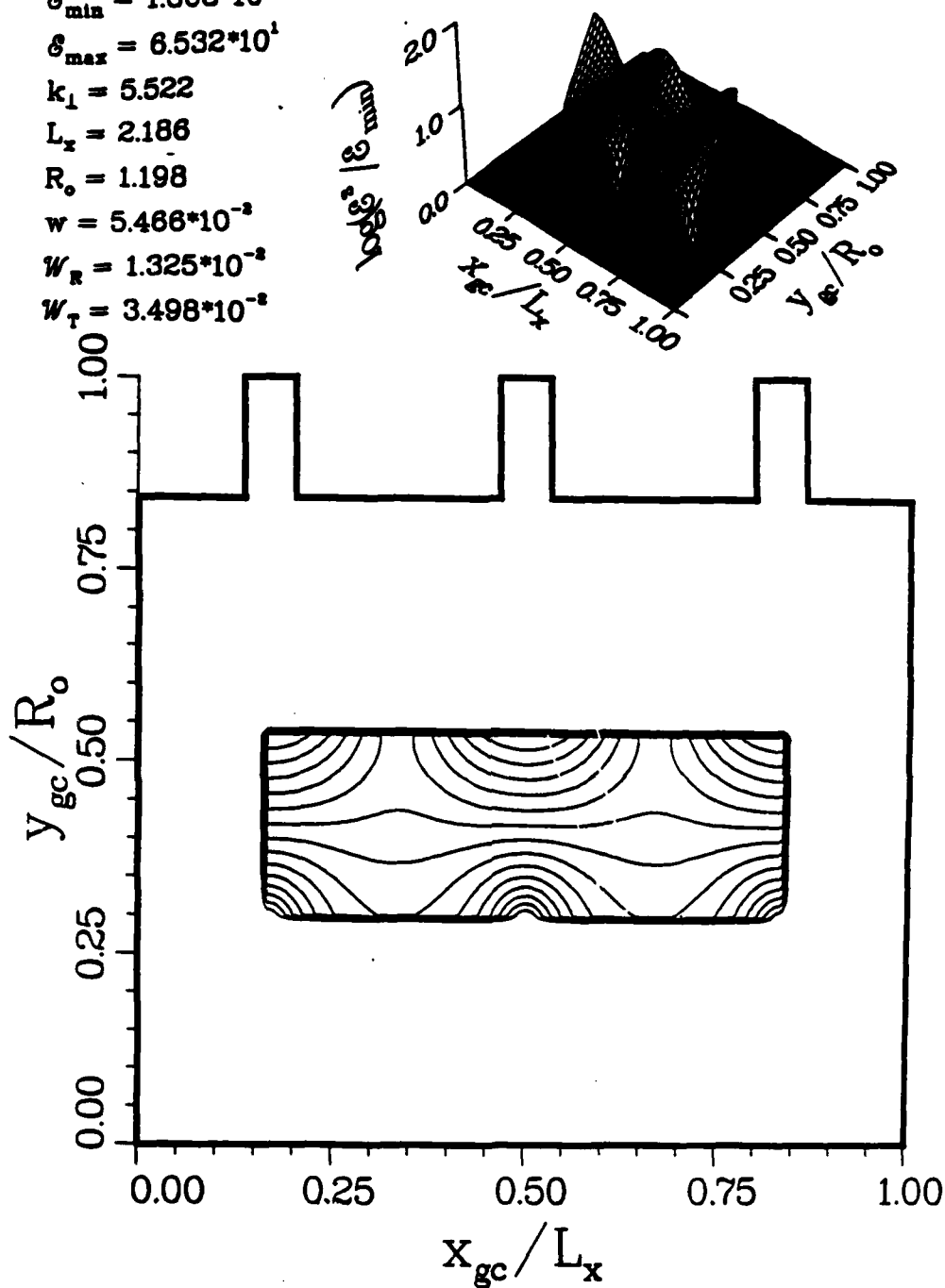
$R_o = 1.198$

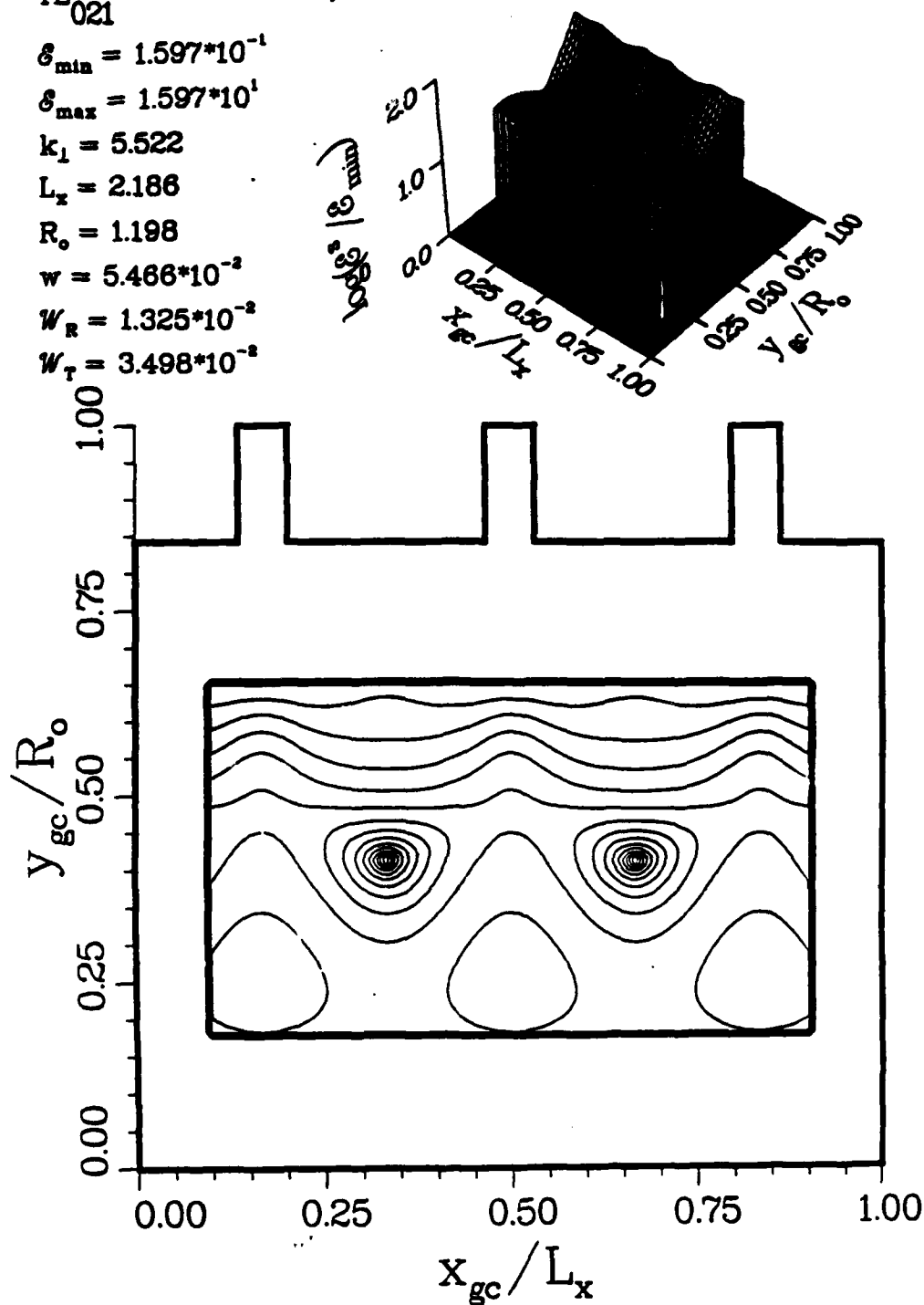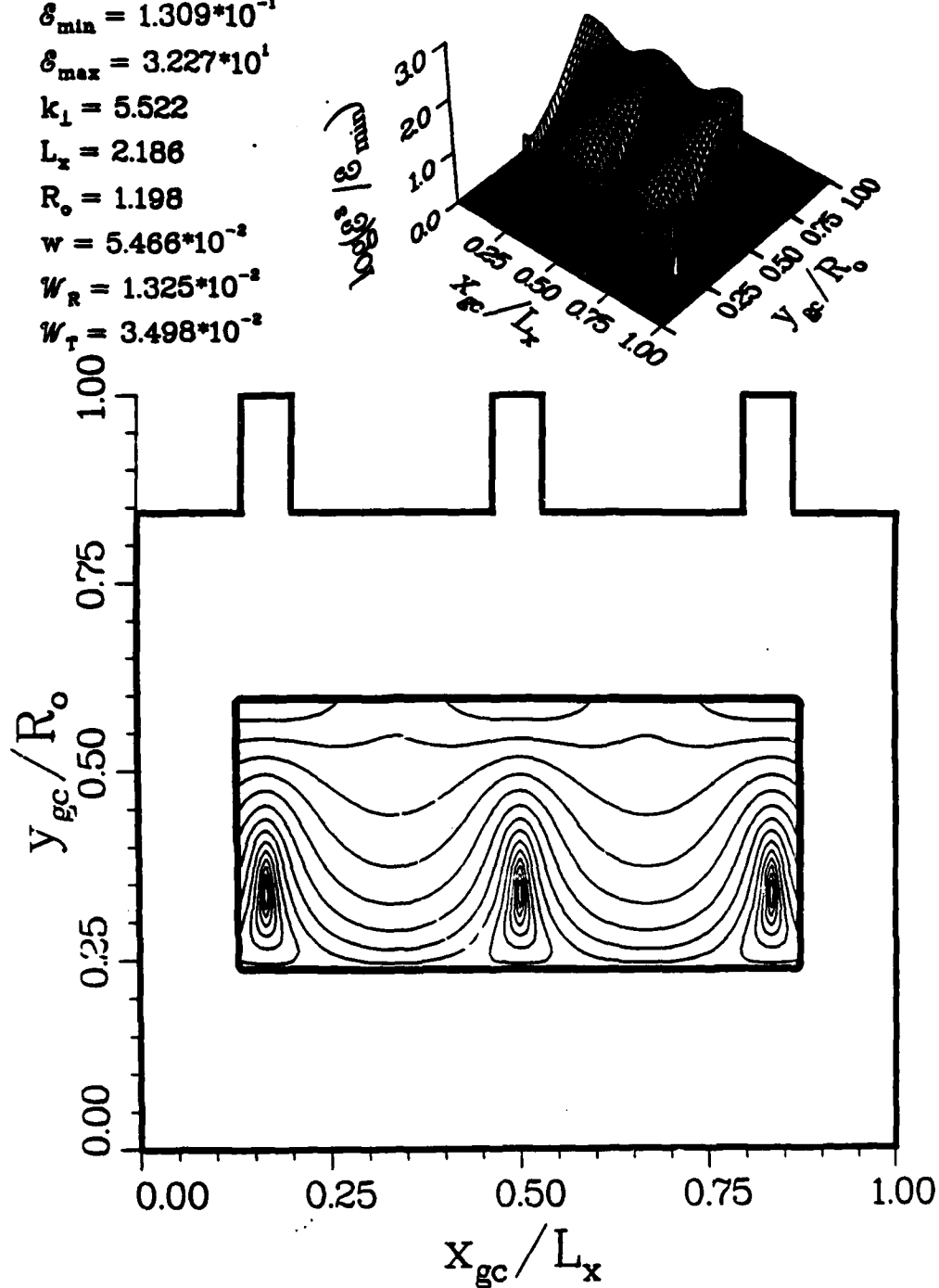$w = 5.466*10^{-2}$

$W_R = 1.325*10^{-2}$

$W_T = 3.498*10^{-2}$

FIG. 4(d). Surface and contour plot for $\mathcal{E}^a$ for $s = 6$. Contours are shown at intervals of $1/15$ of the maximum value of $\mathcal{E}^a$.

48
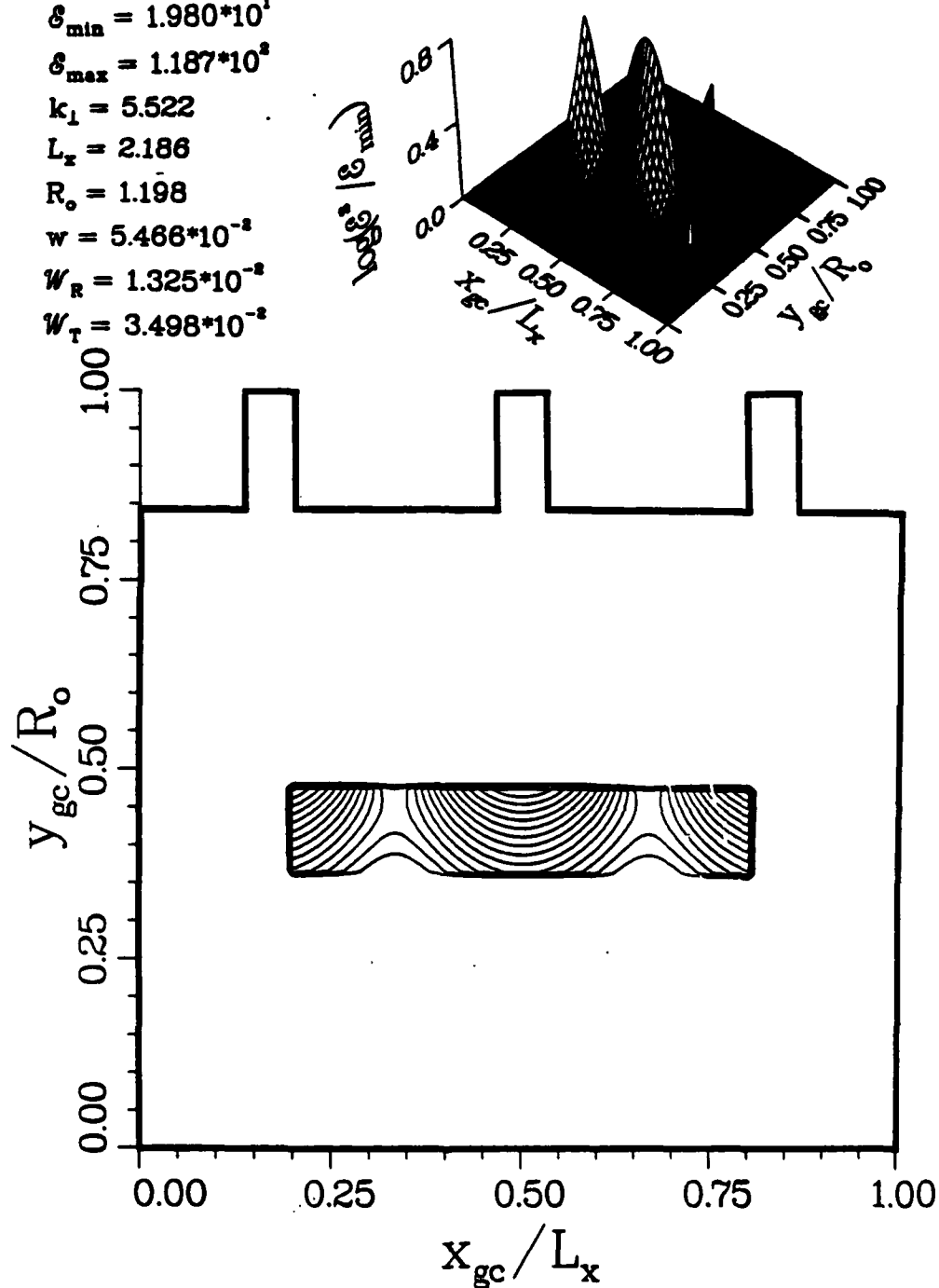
THEORY OF HIGH HARMONIC GYROTRON OSCILLATORS WITH SLOTTED CROSS SECTION STRUCTURE*

P. VITELLO AND C. MENYUK[†]

SCIENCE APPLICATIONS INTERNATIONAL CORPORATION
1710 GOODRIDGE DRIVE
MCLEAN, VIRGINIA 22102 USA

[†] Permanent Address: Department of Electrical Engineering
University of Maryland
Catonsville, MD 21228
and
College Park, MD 20742

49

ABSTRACT

A linear theory analysis of gyrotron oscillators with slotted cross section is used to calculate the net change in beam energy $\langle \delta\gamma \rangle_{t_o \varphi_o}$. In our new formalism, geometric factors are clearly distinguished from the geometry-independent harmonic resonance terms which are due to the fundamental electron cyclotron maser and peniotron interactions. This separation of the interaction terms from the geometric factors greatly simplifies the physical analysis, and leads to a very compact form for $\langle \delta\gamma \rangle_{t_o \varphi_o}$. The theory is applied to slotted rectangular oscillators (which have not previously been treated) and to slotted cylindrical oscillators to show that a unified expression can be obtained for the start oscillation condition. In sample applications of our theory, it is demonstrated that slots lower the start oscillation condition in both cylindrical and rectangular geometries, and can lead to a *decrease* in this condition as harmonic number is increased in the rectangular geometry. The use of these slotted devices thus appears quite attractive in the millimeter wave regime. We also find that the peniotron interaction, *which is easily identified in our formalism,* may be very strong in slotted cavities.

I. Introduction

The gyrotron is well known as a coherent microwave source capable of generating unprecedented power levels. Gyrotron emission occures at harmonics of the electron cyclotron frequency. As the emission frequency increases either large magnetic fields must be used or operation at high cyclotron harmonics is required. Presently, most gyrotron development has focused on devices using either the first or second harmonics [1-3]. These low harmonics necessitate the use of a superconducting magnet if frequencies as high as the millimeter and sub-millimeter wave regimes are to be achieved.

High harmonic gyrotron emission has been achieved for several tube designs. Using smooth walled cylindrical cavities and an axis encircling beam, harmonics as high as $m = 11$ have been observed for a TE_{m1l} "whispering gallery" mode gyrotron oscillator [4-5]. A high energy, large Larmor orbit beam is required for "whispering gallery" mode gyrotrons as these modes tend to concentrate the RF field towards the wall of the cavity. Also using an axis encircling beam with high energy (2 MeV) electrons, Destler et al. [6] have reported the generation of a strong burst of microwave radiation at the 12th harmonic from a slotted cylindrical tube. This new interactive slotted structure leads to an excellent high harmonic interaction and good mode selection. Further investigations of slotted cylindrical tubes [7–15] and of slotted rectangular and ridged rectangular tubes [16–19] has shown that even for moderate beam energies, strong high harmonic fringe fields can be positioned at the beam orbits. Two slotted tube geometries, shown in Figure 1, have been investigated in detail; these are the cylindrical (or magnetron type) geometry, and rectangular geometries, both slotted and ridged. As there is no real distinction between slotted and ridged tubes, we will refer to them all as slotted. Both gyro-TWT amplifiers [7–10] and gyrotron oscillators [11–15] have been studied theoretically in slotted, cylindrical geometries. For rectangular geometries only gyro-TWT amplifiers have been studied in detail for slotted cavities

[16–19]. All of these studies show that slotted structures greatly increase the high harmonic interaction in a gyrotron relative to a smooth wall design.

In this paper we extend the modeling of slotted gyrotron oscillators by presenting a linear kinetic theory applicable to gyrotrons of both rectangular and cylindrical cross section design. In our analysis we calculate the net energy loss of the beam, $\langle \delta\gamma \rangle_{t_o\, \varphi_o}$, which is needed to determine the cavity start oscillation condition and the frequency detuning. We give $\langle \delta\gamma \rangle_{t_o\, \varphi_o}$ as a sum over harmonics in which each harmonic contribution consists of a geometry-independent factor due to the fundamental interactions and a geometry-dependent factor which varies from device to device. The geometry-independent factor consists of clearly distinguished terms due to the electron cyclotron maser and peniotron interactions.

This paper is organized as follows: In §II, we derive the TE mode fields in either rectangular or cylindrical slotted cavities. Two specific examples are presented which are then used in the remainder of the paper. In §III, we present our linear theory and determine the start oscillation condition and frequency detuning of the oscillator cavity modes. In §IV, we present sample calculations which shows both the strong high harmonic content of slotted cavities, and the importance of peniotron emission for these systems.

II. Properties of Slotted Cavity Fields

Let us consider the behavior of the TE modes in a tube with a slotted cross section. If the axial RF magnetic field is written in the form

$$B_z = A_T(x,y)f(z)e^{-i\omega t} \tag{1}$$

(where $f(z) = e^{ik_z z}$ for an amplifier and $f(z) = \sin(k_z z)$ for an oscillator), then from Maxwell's equations [20] the solution for A_T will be an eigenfunction of the equation

$$(\vec{\nabla}_T \cdot \vec{\nabla}_T + k_\perp^2)A_T = 0, \tag{2}$$

subject to the boundary conditions of an assumed perfectly conducting tube wall. In (2), $k_\perp^2 = \omega^2 - k_z^2$ is the transverse wavenumber eigenvalue, and $\vec{\nabla}_T$ is the transverse Laplacian. The transverse RF electric and magnetic fields, $\vec{E}_T$ and $\vec{B}_T$ may be obtained from B_z as follows,

$$\vec{E}_T = -i\frac{\omega}{k_\perp^2}\left(\hat{z} \times \vec{\nabla}_T B_z\right), \tag{3}$$

$$\vec{B}_T = \frac{1}{k_\perp^2}\frac{\partial}{\partial z}\vec{\nabla}_T B_z. \tag{4}$$

Two sets of orthogonal eigenfunction basis sets are commonly used to describe A_T in slotted cavities. If the cross section is naturally specified in a Cartesian coordinate system, then the solution

$$A_T(x,y) = \sum_{\Gamma=-\infty}^{\infty} A_\Gamma \left(e^{-ik_{x\Gamma}x} + a_\Gamma e^{ik_{x\Gamma}x}\right)\left(e^{-ik_{y\Gamma}y} + b_\Gamma e^{ik_{y\Gamma}y}\right), \tag{5}$$

where $k_{x\Gamma}^2 + k_{y\Gamma}^2 = k_\perp^2$, should be used. For a cross section with cylindrical symmetry,

$$A_T(r,\theta) = \sum_{\Gamma=-\infty}^{\infty} A_\Gamma C_\Gamma(k_\perp r)e^{i\Gamma\theta}, \tag{6}$$

should be used. In (6), $C_\Gamma(k_\perp r) = J_\Gamma(k_\perp r) + a_\Gamma Y_\Gamma(k_\perp r)$, where J_Γ and Y_Γ are Bessel functions of the first and second kind. The constants A_Γ, a_Γ, and b_Γ depend on the

53

tube geometry. For both of these eigenfunction basis sets the coordinate dependence is separable. The total time averaged, volume integrated RF field energy stored in the fields, $\mathcal{W}$, can in all cases be written as

$$\mathcal{W} = \frac{1}{16\pi} \int dV \left(\vec{E} \cdot \vec{E}^* + \vec{B} \cdot \vec{B}^* \right). \qquad (7)$$

In calculating $\mathcal{W}$, any static magnetic field energy is not included.

We now consider the RF cavity fields for two specific cases, a slotted co-axial cylindrical cavity as shown in Figure 1a and a slotted rectangular cavity as shown by Figure 1b. We will use N to designate the number of slots and L_x as the axial length of the cavity. In the cylindrical co-axial cavity, the central co-axial radius is given by R_i, while the inner and outer slot radii are respectively R and R_o. The angular width of the slots is taken to be $2\theta_o$. In the rectangular cavity, the inner and outer slot dimensions are R and R_o, while the cavity width in the x direction is given as L_x. The distance $2d$ between the slots equals twice the distance from the first or last slot to the tube wall; the slot width is taken to be $2w$. In the following we make use of dimensionless units, with the cavity transverse length R being our scaling parameter. In these units, length is measured in units of R, time in units of R/c, frequency in units of c/R, and the background magnetic and RF fields are measured in units of $m_e c^2/|e|R$, where m_e is the electron rest mass, e is the electron charge, and c is the speed of light. The dimensionless cyclotron frequency Ω/γ is equal in these units to B_o/γ where B_o is the assumed constant background magnetic field and γ is the relativistic factor.

To determine the RF fields, it it convenient to treat the cavity proper (Region I) and the slots (Region II) as separate expansions which are matched across the slot openings [21]. We take the relative phase dependence of each of the N slots as being $e^{i2\pi mq/N}$ for the cylindrical slotted case and $\cos[\pi(q+1/2)m/N]$ for the rectangular slotted case, where $q = 0, \ldots, N-1$ is the slot number. The value of the mode number m determines the overall mode. The 2π mode corresponds to $m = 0$, while the π mode

is given by $m = N/2$ for a cylindrical slotted cavity, and by $m = N$ for a rectangular

slotted cavity. In order to obtain a closed analytic form for the field solution, an infinite

sum is used only in Region I, with just the $\Gamma = 0$ term being kept in Region II. The RF

fields for the slotted co-axial cylindrical cavity are then given approximately by [12]

Region I

$$E_r = - E_o \frac{\omega}{k_\perp} \sum_{j=-\infty}^{\infty} A_\Gamma^I \left[\frac{\Gamma C_\Gamma^I(k_\perp r)}{k_\perp r} \right] \sin(k_z z) e^{i(\Gamma\theta - \omega t)}, \tag{8}$$

$$E_\theta = -iE_o \frac{\omega}{k_\perp} \sum_{j=-\infty}^{\infty} A_\Gamma^I C_\Gamma^{I\,'}(k_\perp r) \sin(k_z z) e^{i(\Gamma\theta - \omega t)}, \tag{9}$$

$$E_z = \quad 0, \tag{10}$$

$$B_r = \quad E_o \frac{k_z}{k_\perp} \sum_{j=-\infty}^{\infty} A_\Gamma^I C_\Gamma^{I\,'}(k_\perp r) \cos(k_z z) e^{i(\Gamma\theta - \omega t)}, \tag{11}$$

$$B_\theta = \quad iE_o \frac{k_z}{k_\perp} \sum_{j=-\infty}^{\infty} A_\Gamma^I \left[\frac{\Gamma C_\Gamma^I(k_\perp r)}{k_\perp r} \right] \cos(k_z z) e^{i(\Gamma\theta - \omega t)}, \tag{12}$$

$$B_z = \quad E_o \sum_{j=-\infty}^{\infty} A_\Gamma^I C_\Gamma^I(k_\perp r) \sin(k_z z) e^{i(\Gamma\theta - \omega t)}, \tag{13}$$

Region II

$$E_r = 0, \tag{14}$$

$$E_\theta = -iE_o \frac{\omega}{k_\perp} e^{i2\pi mq/N} A_0^{II} C_0^{II'}(k_\perp r) \sin(k_z z) e^{-i\omega t}, \tag{15}$$

$$E_z = 0, \tag{16}$$

$$B_r = E_o \frac{k_z}{k_\perp} e^{i2\pi mq/N} A_0^{II} C_0^{II'}(k_\perp r) \cos(k_z z) e^{-i\omega t}, \tag{17}$$

$$B_\theta = 0, \tag{18}$$

$$B_z = E_o e^{i2\pi mq/N} A_0^{II} C_0^{II}(k_\perp r) \sin(k_z z) e^{-i\omega t}, \tag{19}$$

where

$$A_\Gamma^I = \frac{\sin(\Gamma\theta_o)}{\Gamma} \frac{1}{C_\Gamma^{I'}(k_\perp)}, \tag{20}$$

$$A_0^{II} = \frac{\pi}{N} \frac{1}{C_0^{II'}(k_\perp)}, \tag{21}$$

and

$$C_\Gamma^I(k_\perp r) = J_\Gamma(k_\perp r) - J_\Gamma'(k_\perp R_i) Y_\Gamma(k_\perp r) / Y_\Gamma'(k_\perp R_i), \tag{22}$$

$$C_0^{II}(k_\perp r) = J_0(k_\perp r) - J_0'(k_\perp R_o) Y_0(k_\perp r) / Y_0'(k_\perp R_o). \tag{23}$$

A prime represents differentiation with respect to the argument. Due to the cavity symmetry, the only harmonics which contribute are $\Gamma = m + jN$, where $j = 0, \pm 1, \pm 2, \ldots$ For these fields, the dispersion relation determining $k_\perp$, and the total field energy $\mathcal{W}$ are

$$\frac{N\theta_o}{\pi} \sum_{j=-\infty}^{\infty} \left(\frac{\sin\Gamma\theta_o}{\Gamma\theta_o}\right)^2 \frac{C_\Gamma^I(k_\perp)}{C_\Gamma^{I'}(k_\perp)} = \frac{C_0^{II}(k_\perp)}{C_0^{II'}(k_\perp)}, \tag{24}$$

56

and

$$W = \frac{\omega^2 L_z}{k_\perp^2 16}\left\{\sum_{j=-\infty}^{\infty} [A_\Gamma^I]^2 \left[[C_\Gamma^I(k_\perp)]^2\left(1-\frac{\Gamma^2}{k_\perp^2}\right) - R_i^2\,[C_\Gamma^I(k_\perp R_i)]^2\left(1-\frac{\Gamma^2}{k_\perp^2 R_i^2}\right)\right.\right.$$

$$\left. + \left[C_\Gamma^{I\prime}(k_\perp)\right]^2 + \frac{1}{k_\perp}C_\Gamma^{I\prime}(k_\perp)C_\Gamma^I(k_\perp)\left(1+\frac{k_z^2}{\omega^2}\right)\right]$$

$$+ \frac{N\theta_o\,[A_0^{II}]^2}{\pi}\left[R_o^2\,[C_0^{II}(k_\perp R_o)]^2 - [C_0^{II}(k_\perp)]^2\right.$$

$$\left.\left. - \left[C_0^{II\prime}(k_\perp)\right]^2 - \frac{1}{k_\perp}C_0^{II\prime}(k_\perp)C_0^{II}(k_\perp)\left(1+\frac{k_z^2}{\omega^2}\right)\right]\right\}. \tag{25}$$

The slight difference between W as given in (25) and the form presented by Chu and Dialetis [11–12] stems from our use of the field energy density $\vec{E}\cdot\vec{E}^* + \vec{B}\cdot\vec{B}^*$ while Chu and Dialetis used $2\vec{E}\cdot\vec{E}^*$. If the RF fields were calculated exactly, with an infinite series expansion for both Regions I and II, then the energy in the magnetic fields would equal that in the electric fields and both expressions for W would be identical.

The rectangular slotted fields (see, e.g. [18] for a derivation) for our tube are

Region I

$$E_x = -i\frac{\omega}{k_\perp^2}E_o\sum_\Gamma k_{y_\Gamma}A_\Gamma^I\cos(k_{x_\Gamma}x)\sin(k_{y_\Gamma}y)\sin(k_z z)e^{-i\omega t}, \tag{26}$$

$$E_y = \quad i\frac{\omega}{k_\perp^2}E_o\sum_\Gamma k_{x_\Gamma}A_\Gamma^I\sin(k_{x_\Gamma}x)\cos(k_{y_\Gamma}y)\sin(k_z z)e^{-i\omega t}, \tag{27}$$

$$E_z = \quad 0, \tag{28}$$

$$B_x = -\frac{k_z}{k_\perp^2}E_o\sum_\Gamma k_{x_\Gamma}A_\Gamma^I\sin(k_{x_\Gamma}x)\cos(k_{y_\Gamma}y)\cos(k_z z)e^{-i\omega t}, \tag{29}$$

$$B_y = -\frac{k_z}{k_\perp^2}E_o\sum_\Gamma k_{y_\Gamma}A_\Gamma^I\cos(k_{x_\Gamma}x)\sin(k_{y_\Gamma}y)\cos(k_z z)e^{-i\omega t}, \tag{30}$$

$$B_z = \quad E_o\sum_\Gamma A_\Gamma^I\cos(k_{x_\Gamma}x)\cos(k_{y_\Gamma}y)\sin(k_z z)e^{-i\omega t}, \tag{31}$$

57

Region II

$$E_x = -i\frac{\omega}{k_\perp}E_o \cos(\pi(q+1/2)m/N)\mathcal{A}_0^{II} \sin(k_\perp y)\sin(k_z z)e^{-i\omega t}, \quad (32)$$

$$E_y = \quad 0, \quad (33)$$

$$E_z = \quad 0, \quad (34)$$

$$B_x = \quad 0, \quad (35)$$

$$B_y = -\frac{k_z}{k_\perp}E_o \cos(\pi(q+1/2)m/N)\mathcal{A}_0^{II} \sin(k_\perp y)\cos(k_z z)e^{-i\omega t}, \quad (36)$$

$$B_z = \quad E_o \cos(\pi(q+1/2)m/N)\mathcal{A}_0^{II} \cos(k_\perp y)\sin(k_z z)e^{-i\omega t}, \quad (37)$$

where, $k_{x_\Gamma} = \Gamma\pi/L_x$, $k_{y_\Gamma} = \left(k_\perp^2 - k_{x_\Gamma}^2\right)^{1/2}$, and

$$\mathcal{A}_\Gamma^I = \frac{2k_\perp^2 \sin(k_{x_\Gamma} w)(-1)^j}{(1+\delta_{\Gamma 0})\, k_{x_\Gamma}\, k_{y_\Gamma} \sin(k_{y_\Gamma})}, \quad (38)$$

$$\mathcal{A}_0^{II} = \frac{k_\perp L_x}{N \sin\left[k_\perp(1-R_o)\right]}. \quad (39)$$

Only $\Gamma = \pm m + 2Nj$, $j = 0,1,2,\ldots$, with $\Gamma \geq 0$ are to be included in the sums. For $m = 0$, each term for $\Gamma = 2Nj$ must be counted twice. For our model of a rectangular slotted cavity, the RF field in Region I is not affected by the presence of the slots for the modes $m = Ni$, where $i = 1,3,5,\ldots$, and has the same form as in a simple smooth walled cavity. For all other rectangular cavity modes, the dispersion relation for $k_\perp$ and volume integrated energy $\mathcal{W}$ can be written as

$$\frac{2Nw}{L_x}\sum_\Gamma \frac{k_\perp}{1+\delta_{\Gamma 0}}\cdot\left[\frac{\sin(k_{x_\Gamma} w)}{k_{x_\Gamma} w}\right]^2 \frac{\cot(k_{y_\Gamma})}{k_{y_\Gamma}} = \cot\left[k_\perp(1-R_o)\right], \quad (40)$$

and

$$\mathcal{W} = \frac{L_z L_z \omega^2 (1+\delta_{m0})}{64\pi k_\perp^2}\left(\sum_\Gamma \left(\mathcal{A}_\Gamma^I\right)^2 (1+\delta_{\Gamma 0})\left\{1 + \frac{\sin(2k_{y_\Gamma})}{4k_{y_\Gamma}}\left[\frac{k_\perp^2}{\omega^2} + \left(1+\frac{k_z^2}{\omega^2}\right)\left(\frac{2k_{x_\Gamma}^2}{k_\perp^2}-1\right)\right]\right\}\right.$$
$$\left. + \frac{2Nw(R_o-1)\left(\mathcal{A}_0^{II}\right)^2}{L_x}\left[1 + \frac{\sin(2k_\perp(1-R_o))}{4k_\perp(1-R_o)}\left(\frac{k_\perp^2}{\omega^2}-1-\frac{k_z^2}{\omega^2}\right)\right]\right). \quad (41)$$

58

III. Linear Kinetic Theory

To solve for the interaction of the electron beam with the RF field we use the single particle relativistic equation of motion

$$\frac{d\vec{U}}{dz} = -\frac{\gamma}{U_z}\left[\vec{E} + \frac{\vec{U} \times \vec{B}}{\gamma}\right],\tag{42}$$

where $\vec{U} = \gamma\vec{\beta}$ is the product of the electron velocity $\vec{\beta}$ and the Lorentz factor γ. Note that we are using time, $t(z)$, as a dependent variable, and the axial position z as the independent variable. The use of z facilitates the comparison of the linear theory with the weak field limit of a nonlinear numerical modeling of the equations of motion. In dimensionless units, $\gamma = (1 + \vec{U} \cdot \vec{U})^{1/2} = (1 + U_z^2 + U_\perp^2)^{1/2}$ gives the electron energy. From (42) it follows that the change in γ is

$$\frac{d\gamma}{dz} = -\frac{\vec{U} \cdot \vec{E}}{U_z}.\tag{43}$$

Regardless of the symmetry of the overall cavity fields, the guiding center coordinates (see Figure 2) are the natural system to use when carrying our linear theory. The guiding center variables may be expressed as $(U_\perp, U_z, \varphi, x_{gc}, y_{gc}, t)$ in Cartesian coordinates or $(U_\perp, U_z, \varphi, r_{gc}, \psi_{gc}, t)$ in cylindrical coordinates. The guiding center coordinates are related to cavity frame coordinates by the relations

$$x = x_{gc} + r_L \cos(\varphi)$$

$$= r_{gc} \cos(\psi_{gc}) + r_L \cos(\varphi),\tag{44}$$

$$y = y_{gc} + r_L \sin(\varphi)$$

$$= r_{gc} \sin(\psi_{gc}) + r_L \sin(\varphi),\tag{45}$$

$$U_x = -U_\perp \sin(\varphi),\tag{46}$$

$$U_y = U_\perp \cos(\varphi).\tag{47}$$

59

The position (x_{gc}, y_{gc}) or (r_{gc}, ψ_{gc}) corresponds to the electron guiding center position, with $r_L = U_\perp / B_o$ being the Larmor radius. The dynamical equations for the guiding center variables follow from (42, 44–47),

$$\frac{dU_\perp}{dz} = -\frac{\gamma}{U_z} \left[E_\varphi + U_z B_{r_L} / \gamma \right], \tag{48}$$

$$\frac{d\varphi}{dz} = \frac{\gamma}{U_z U_\perp} \left[E_{r_L} - U_z B_\varphi / \gamma + U_\perp B_z / \gamma \right] + \frac{B_o}{U_z}, \tag{49}$$

$$\frac{dU_z}{dz} = \frac{U_\perp}{U_z} B_{r_L}, \tag{50}$$

$$\frac{dt}{dz} = \frac{\gamma}{U_z}, \tag{51}$$

and either

$$\frac{dx_{gc}}{dz} = \frac{\gamma}{U_z B_o} \left[(E_\varphi + U_z B_{r_L} / \gamma) \cos(\varphi) \right.$$
$$\left. + (E_{r_L} - U_z B_\varphi / \gamma + U_\perp B_z / \gamma) \sin(\varphi) \right], \tag{52}$$

$$\frac{dy_{gc}}{dz} = \frac{\gamma}{U_z B_o} \left[(E_\varphi + U_z B_{r_L} / \gamma) \sin(\varphi) \right.$$
$$\left. - (E_{r_L} - U_z B_\varphi / \gamma + U_\perp B_z / \gamma) \cos(\varphi) \right], \tag{53}$$

or

$$\frac{dr_{gc}}{dz} = \frac{\gamma}{U_z B_o} \left[(E_\varphi + U_z B_{r_L} / \gamma) \cos(\psi_{gc} - \varphi) \right.$$
$$\left. - (E_{r_L} - U_z B_\varphi / \gamma + U_\perp B_z / \gamma) \sin(\psi_{gc} - \varphi) \right], \tag{54}$$

$$\frac{d\psi_{gc}}{dz} = -\frac{\gamma}{r_{gc} U_z B_o} \left[(E_\varphi + U_z B_{r_L} / \gamma) \sin(\psi_{gc} - \varphi) \right.$$
$$\left. + (E_{r_L} - U_z B_\varphi / \gamma + U_\perp B_z / \gamma) \cos(\psi_{gc} - \varphi) \right]. \tag{55}$$

The RF fields terms, E_φ, E_{r_L}, B_φ, and B_{r_L}, correspond to the values of $\vec{E}$ and $\vec{B}$ along the $\hat{\varphi}$ and $\hat{r}_L$ directions.

To solve for the perturbations induced by the RF field, we linearize the equations of motion as follows

$$U_\perp = U_{\perp_o} + \delta U_\perp, \tag{56}$$

$$U_z = U_{z_o} + \delta U_z, \tag{57}$$

$$\varphi = \varphi_o + B_o \frac{(z - z_o)}{U_{z_o}} + \delta\varphi, \tag{58}$$

$$x_{gc} = x_{gc_o} + \delta x_{gc}, \tag{59}$$

$$y_{gc} = y_{gc_o} + \delta y_{gc}, \tag{60}$$

$$r_{gc} = r_{gc_o} + \delta r_{gc}, \tag{61}$$

$$\psi_{gc} = \psi_{gc_o} + \delta\psi_{gc}, \tag{62}$$

$$t = t_o + \frac{\gamma_o(z - z_o)}{U_{z_o}} + \delta t, \tag{63}$$

where the constants $U_{\perp_o}$, U_{z_o}, φ_o, x_{gc_o}, y_{gc_o}, r_{go_o}, ψ_{gc_o}, and t_o represent the initial variable values at the entrance position of the cavity z_o. In the following we take $z_o = 0$. The equations of motion for the perturbed variables then follow as

$$\frac{d\delta U_\perp}{dz} = -\frac{\gamma_o}{U_{z_o}} \tilde{E}_\varphi^o, \tag{64}$$

$$\frac{d\delta\varphi}{dz} = \frac{\gamma_o}{U_{z_o} U_{\perp_o}} \tilde{E}_{r_L}^o - B_o \frac{\delta U_z}{U_{z_o}^2}, \tag{65}$$

$$\frac{d\delta U_z}{dz} = \frac{U_{\perp_o}}{U_{z_o}} B_{r_L}^o, \tag{66}$$

$$\frac{d\delta t}{dz} = -\frac{1}{\gamma_o U_{z_o}} \left[\frac{1 + U_{\perp_o}^2}{U_{z_o}} \delta U_z - U_{\perp_o} \delta U_{\perp_o} \right], \tag{67}$$

$$\frac{\mathrm{d}\delta x_{gc}}{\mathrm{d}z} = \frac{\gamma_o}{U_{z_o} B_o} \left[\tilde{E}^o_\varphi \cos(\phi_o) + \tilde{E}^o_{r_L} \sin(\phi_o) \right], \tag{68}$$

$$\frac{\mathrm{d}\delta y_{gc}}{\mathrm{d}z} = \frac{\gamma_o}{U_{z_o} B_o} \left[\tilde{E}^o_\varphi \sin(\phi_o) - \tilde{E}^o_{r_L} \cos(\phi_o) \right], \tag{69}$$

$$\frac{\mathrm{d}\delta r_{gc}}{\mathrm{d}z} = \frac{\gamma_o}{U_{z_o} B_o} \left[\tilde{E}^o_\varphi \cos(\psi_{gc_o} - \phi_o) - \tilde{E}^o_{r_L} \sin(\psi_{gc_o} - \phi_o) \right], \tag{70}$$

$$\frac{\mathrm{d}\delta \psi_{gc}}{\mathrm{d}z} = -\frac{\gamma_o}{U_{z_o} B_o r_{gc_o}} \left[\tilde{E}^o_\varphi \sin(\psi_{gc_o} - \phi_o) + \tilde{E}^o_{r_L} \cos(\psi_{gc_o} - \phi_o) \right], \tag{71}$$

where

$$\tilde{E}^o_\varphi = E^o_\varphi + U_{z_o} B^o_{r_L}/\gamma_o, \tag{72}$$

$$\tilde{E}^o_{r_L} = E^o_{r_L} - U_{z_o} B^o_\varphi/\gamma_o + U^o_\perp B^o_z/\gamma_o, \tag{73}$$

$$\phi_o = \varphi_o + B_o z/U_{z_o}. \tag{74}$$

E^o_φ, $E^o_{r_L}$, B^o_φ, $B^o_{r_L}$, and B^o_z are the RF field terms in the $\hat\varphi$, $\hat{r}_L$, and $\hat{z}$ directions evaluated along the unperturbed orbits. $\tilde{E}^o_\varphi$ and $\tilde{E}^o_{r_L}$ represent respectively the $\hat\varphi$ and $\hat{r}_L$ components of vector $\vec{E} + \vec{U} \times \vec{B}/\gamma$ from the equation of motion also evaluated along the unperturbed orbits. The variable ϕ_o gives the phase variation about the guiding center for zero RF field.

To calculate the average change in energy for the beam we must also linearize the energy equation (43), which becomes

$$\frac{\mathrm{d}\delta\gamma}{\mathrm{d}z} = -\frac{\delta U_\perp}{U_{z_o}} E^{o\,*}_\varphi + \frac{U_{\perp_o} \delta U_z}{U^2_{z_o}} E^{o\,*}_\varphi - \frac{U_{\perp_o}}{U_{z_o}} \left[\delta t \frac{\partial E^{o\,*}_\varphi}{\partial t} + \delta r_{gc} \frac{\partial E^{o\,*}_\varphi}{\partial r_{gc}} \right.$$
$$\left. + \delta\psi_{gc} \frac{\partial E^{o\,*}_\varphi}{\partial\psi_{gc}} + \delta r_L \frac{\partial E^{o\,*}_\varphi}{\partial r_L} + \delta\varphi \frac{\partial E^{o\,*}_\varphi}{\partial\varphi} \right]. \tag{75}$$

or

$$\frac{\mathrm{d}\delta\gamma}{\mathrm{d}z} = -\frac{\delta U_\perp}{U_{z_o}} E^{o\,*}_\varphi + \frac{U_{\perp_o} \delta U_z}{U^2_{z_o}} E^{o\,*}_\varphi - \frac{U_{\perp_o}}{U_{z_o}} \left[\delta t \frac{\partial E^{o\,*}_\varphi}{\partial t} + \delta x_{gc} \frac{\partial E^{o\,*}_\varphi}{\partial x_{gc}} \right.$$
$$\left. + \delta y_{gc} \frac{\partial E^{o\,*}_\varphi}{\partial y_{gc}} + \delta r_L \frac{\partial E^{o\,*}_\varphi}{\partial r_L} + \delta\varphi \frac{\partial E^{o\,*}_\varphi}{\partial\varphi} \right]. \tag{76}$$

For a constant background magnetic field B_o, $\delta r_L = \delta U_\perp / B_o$. The equations for $d\delta\gamma/dz$ have been expanded to second order in the RF field amplitude E_o.

In order to solve these linearized equations we must express the RF fields in terms of the guiding center coordinates. For the cylindrical geometry eigenfunction set (8–13) Graf's theorem [22],

$$C_\nu(k_\perp r) {\cos \atop \sin} \nu(\psi_{gc} - \theta) = \sum_{k=-\infty}^{\infty} C_{\nu+k}(K_{gc}) J_k(K_L) {\cos \atop \sin} k(\pi - \psi_{gc} + \varphi), \qquad (77)$$

for $r_{gc} > r_L$, or

$$C_\nu(k_\perp r) {\cos \atop \sin} \nu(\psi_{gc} - \theta) = \sum_{k=-\infty}^{\infty} {}' J_{\nu+k}(K_{gc}) C_k(K_L) {\cos \atop \sin} k(\pi - \psi_{gc} + \varphi), \qquad (78)$$

for $r_{gc} < r_L$, is used where $K_{gc} = k_\perp r_{gc}$ and $K_L = k_\perp r_L$. For the rectangular geometry eigenfunction set (26–31), the expansions

$$\cos\left[K_L \sin(\varphi \pm \lambda)\right] = \sum_{k=-\infty}^{\infty} J_k(K_L) \cos\left[k(\varphi \pm \lambda)\right], \qquad (79)$$

$$\sin\left[K_L \sin(\varphi \pm \lambda)\right] = \sum_{k=-\infty}^{\infty} J_k(K_L) \sin\left[k(\varphi \pm \lambda)\right], \qquad (80)$$

$$\cos\left[K_L \cos(\varphi \pm \lambda)\right] = \sum_{k=-\infty}^{\infty} J_k(K_L) \cos\left[k(\varphi \pm \lambda + \pi/2)\right], \qquad (81)$$

$$\sin\left[K_L \cos(\varphi \pm \lambda)\right] = \sum_{k=-\infty}^{\infty} J_k(K_L) \sin\left[k(\varphi \pm \lambda + \pi/2)\right], \qquad (82)$$

are similarly used. In (79–82), $\cos\lambda = k_x/k_\perp$.

Using the above expansions, the guiding center RF fields in Region I which contains

63

the beam can be expressed as

$$E_{r_L} = -\frac{\omega}{k_\perp} E_o \sum_\Gamma A_\Gamma^I \sum_{s=-\infty}^{\infty} \mathcal{D}_{\Gamma s} \left(\frac{s J_s(K_L)}{K_L} \right) \sin(k_z z) e^{i(s\varphi - \omega t)}, \qquad (83)$$

$$E_\varphi = -i\frac{\omega}{k_\perp} E_o \sum_\Gamma A_\Gamma^I \sum_{s=-\infty}^{\infty} \mathcal{D}_{\Gamma s} J_s'(K_L) \sin(k_z z) e^{i(s\varphi - \omega t)}, \qquad (84)$$

$$B_{r_L} = \frac{k_z}{\omega} E_o \sum_\Gamma A_\Gamma^I \sum_{s=-\infty}^{\infty} \mathcal{D}_{\Gamma s} J_s'(K_L) \cos(k_z z) e^{i(s\varphi - \omega t)}, \qquad (85)$$

$$B_\varphi = i\frac{k_z}{\omega} E_o \sum_\Gamma A_\Gamma^I \sum_{s=-\infty}^{\infty} \mathcal{D}_{\Gamma s} \left(\frac{s J_s(K_L)}{K_L} \right) \cos(k_z z) e^{i(s\varphi - \omega t)}, \qquad (86)$$

$$B_z = E_o \sum_\Gamma A_\Gamma^I \sum_{s=-\infty}^{\infty} \mathcal{D}_{\Gamma s} J_s(K_L) \sin(k_z z) e^{i(s\varphi - \omega t)}, \qquad (87)$$

where the function $\mathcal{D}_{\Gamma s}$ is

$$\mathcal{D}_{\Gamma s} = C_{\Gamma-s}^I (K_{gc}) e^{i(\Gamma-s)\psi_{gc}} \qquad (88)$$

for the cylindrical coordinates eigenfunction expansion, and

$$\mathcal{D}_{\Gamma s} = \frac{1}{2} \left[e^{ik_{x_\Gamma} x_{gc}} \cos(k_{y_\Gamma} y_{gc} - s\lambda_\Gamma) + (-1)^s e^{-ik_{x_\Gamma} x_{gc}} \cos(k_{y_\Gamma} y_{gc} + s\lambda_\Gamma) \right] e^{is\pi/2} \qquad (89)$$

for the Cartesian coordinates expansion. For cylindrical coordinates, if $r_L > r_{gc}$, the replacement $C^I \to J$ and $J \to C^I$ must be made in (83–88). The form of the guiding center RF fields is clearly independent of the choice of the coordinate eigenfunction basis set one wishes to use to describe the cavity fields and follows from the Fourier transformation for our separable eigenfunction expansion. To determine the contribution of the cavity field at the sth harmonic, one merely sums the contribution from each Γ eigenfunction $A_\Gamma^I \mathcal{D}_{\Gamma s}$.

When evaluated along the unperturbed particle orbits the only variation in the guiding center RF fields (83–87) comes from $\sin(k_z z) e^{i(s\varphi - \omega t)}$, which takes the simple form $\left(e^{ik_z z} - e^{-ik_z z} \right) e^{i(s B_o/\gamma_o - \omega)\gamma_o z/U_{x_o}} e^{i(s\varphi_o - \omega t_o)}/2i$, making the linearized equations of motion simple to evaluate. These equations are solved in the following order:

64

We first integrate (64, 66, 68–69) or (64, 66, 70–71) to determine $\delta U_\perp$, δU_z, and either δx_{gc} and δy_{gc} or δr_{gc} and $\delta \psi_{gc}$. The expressions for $\delta U_\perp$ and δU_z are then substituted into (65, 67) to determine $\delta \varphi$ and δt. Using these perturbed orbital variables, (75) or (76) is finally integrated from $z = 0$ to $z = L$ in order to calculate $\delta \gamma$. The perturbed energy change is then averaged over t_o and the phase angle φ_o. We will not average over guiding center position at this point. The averaged form for $\langle \delta \gamma \rangle_{t_o \varphi_o}$, which comes from a straight forward integration of (75) or (76) is given by

$$\langle \delta \gamma \rangle_{t_o \varphi_o} = -\frac{E_o^2 \gamma_o \omega^2}{8 U_{z_o}^2 k_\perp^2} \sum_\Gamma \sum_\Lambda \mathcal{A}_\Gamma^{I\,*} \mathcal{A}_\Lambda^I \sum_{s=-\infty}^{\infty} (\alpha_1 + \alpha_2 + \alpha_3 + \alpha_4), \qquad (90)$$

where

$$\alpha_1 = \frac{U_{\perp_o}^2 L_z^3}{\gamma_o U_{z_o} \omega \mu_-^3} \left(\omega^2 - k_z^2\right) \left[i\mu_- \left(e^{i\mu_-} + 1\right) - 2\left(e^{i\mu_-} - 1\right)\right] H_{\Gamma \Lambda s}$$

$$- \frac{U_{\perp_o}^2 L_z^2 k_z}{\gamma_o U_{z_o} \omega \mu_-^2} \left[i\mu_- e^{i\mu_-} - e^{i\mu_-} + 1\right] H_{\Gamma \Lambda s}$$

$$- \frac{L_z^2}{\omega \mu_-^2} \left(i\mu_- - e^{i\mu_-} + 1\right) \left[\left(\omega - k_z U_{z_o}/\gamma_o\right) T_{\Gamma \Lambda s} - k_\perp U_{\perp_o} U_{\Gamma \Lambda s}/\gamma_o\right], \quad (91)$$

$$\alpha_4 = -\frac{U_{\perp_o}^2 L_z^3}{\gamma_o U_{z_o} \omega \mu_- \mu_+^2} \left(\omega^2 - k_z^2\right) \left[\left(i\mu_- e^{i\mu_-} - e^{i\mu_-} + 1\right) \frac{\mu_+}{\mu_-} - e^{i\mu_-} + 1\right] H_{\Gamma \Lambda s}$$

$$- \frac{U_{\perp_o}^2 L_z^2 k_z}{\gamma_o U_{z_o} \omega \mu_-^2} \left[i\mu_- e^{i\mu_-} - e^{i\mu_-} + 1\right] H_{\Gamma \Lambda s}$$

$$- \frac{L_z^2}{\omega \mu_+ \mu_-} \left(e^{i\mu_-} - 1\right) \left[\left(\omega + k_z U_{z_o}/\gamma_o\right) T_{\Gamma \Lambda s} - k_\perp U_{\perp_o} U_{\Gamma \Lambda s}/\gamma_o\right], \qquad (92)$$

$$\mu_\pm = \left(\omega - s B_o/\gamma_o \pm k_z U_{z_o}/\gamma_o\right) L_z \gamma_o / U_{z_o}, \qquad (93)$$

65

and

$$H_{\Gamma \Lambda s} = D_{\Gamma_s}^* D_{\Lambda_s} \left[J_s' \left(K_{L_o} \right) \right]^2 , \tag{94}$$

$$T_{\Gamma \Lambda s} = H_{\Gamma \Lambda s} + K_{L_o} J_s' \left(K_{L_o} \right) \left\{ J_s'' \left(K_{L_o} \right) D_{\Gamma_s}^* D_{\Lambda_s} \right.$$
$$\left. - J_s \left(K_{L_o} \right) \frac{\left[D_{\Gamma_{s+1}}^* D_{\Lambda_{s+1}} + D_{\Gamma_{s-1}}^* D_{\Lambda_{s-1}} \right]}{2} + \frac{s^2 J_s \left(K_{L_o} \right) D_{\Gamma_s}^* D_{\Lambda_s}}{K_o^2} \right\}, \tag{95}$$

$$U_{\Gamma \Lambda s} = -\frac{K_{L_o} J_s' \left(K_{L_o} \right)}{2} \left\{ J_{s-1} \left(K_{L_o} \right) \left[D_{\Gamma_{s-1}}^* D_{\Lambda_{s-1}} - D_{\Gamma_s}^* D_{\Lambda_s} \right] \right.$$
$$\left. + J_{s+1} \left(K_{L_o} \right) \left[D_{\Gamma_{s+1}}^* D_{\Lambda_{s+1}} - D_{\Gamma_s}^* D_{\Lambda_s} \right] \right\}. \tag{96}$$

The functions α_2 and α_3 are related to α_1 and α_4 by

$$\alpha_2 \left(k_z \right) = \alpha_1 \left(-k_z \right), \tag{97}$$

$$\alpha_3 \left(k_z \right) = \alpha_4 \left(-k_z \right). \tag{98}$$

Equation (90) for $\langle \delta \gamma \rangle_{t_o \varphi_o}$ contains a double sum over the cavity mode harmonics Γ and Λ. For the cylindrical coordinates expansion, Γ and Λ are restricted to: $\Gamma = Nj + m$ for $j = 0, \pm 1, \pm 2, \ldots$ and $\Lambda = Nk + m$ for $k = 0, \pm 1, \pm 2, \ldots$. For the Cartesian coordinates expansion, the non-negative harmonics which satisfy $\Gamma = 2Nj \pm m$, where $j = 0, 1, 2, \ldots$, and $\Lambda = 2Nk \pm m$, where $k = 0, 1, 2, \ldots$, are allowed. When $m = 0$, the two Cartesian Γ cavity mode harmonics $\Gamma = 2Nj + m$ and $\Gamma = 2Nj - m$, and the two Λ cavity mode harmonics $\Lambda = 2Nk + m$ and $\Lambda = 2Nk - m$ are identical. In this case, the sums over Γ or Λ can be written as twice the sum for all $\Gamma = 2Nj$ or $\Lambda = 2Nk$. Note again that for the cylindrical expansion, if $r_{L_o} > r_{gc_o}$ one must make the replacement $C^I \rightarrow J$ and $J \rightarrow C^I$ in the above relations.

In (90), the variation of $\langle \delta \gamma \rangle_{t_o \varphi_o}$ with guiding center position only enters through the factors $D_{\Gamma_s}^* D_{\Lambda_s}$, $D_{\Gamma_{s+1}}^* D_{\Lambda_{s+1}}$, and $D_{\Gamma_{s-1}}^* D_{\Lambda_{s-1}}$. Averaging over the guiding center position ψ_{gc_o} from 0 to π for the cylindrical case or x_{gc_o} from 0 to L_x for the

66

Cartesian coordinate case collapses the double sum over Γ and Λ to a single sum with $\Gamma = \Lambda$ and $D_{\Gamma k} D_{\Gamma k}^*$ replaced by either $[C_{\Gamma-k}^I]^2$ or $[\cos(k_{y\Gamma} y_{gc_o})^2 \cos(s\lambda_\Gamma)^2 + \sin(k_{y\Gamma} y_{gc_o})^2 \sin(s\lambda_\Gamma)^2]/2$. For the cylindrical slotted gyrotron oscillator, the resulting expression for $\langle \delta\gamma \rangle_{t_o \varphi_o \psi_{gc_o}}$ agrees with the results of Chu and Dialetis [11–12]. While this guiding center averaging is reasonable for modeling an axis-symmetric beam in a cylindrical cavity, it is not reasonable in a rectangular cavity, where x_{gc_o} cannot realistically be taken within r_{L_o} of the cavity walls. If $m = 2Ni$ where $i = 0, 1, 2, \ldots$, then the RF field shows a N-fold periodicity in the x direction and the simplifying x_{gc_o} averaging can be done from $L_x(j/N)$ to $L_x(k/N)$, where $0 < j < N - 1$, and $j < k < N$.

The form of $\langle \delta\gamma \rangle_{t_o \varphi_o}$ given in (90) is a very complicated function of the beam and cavity parameters. It is far from the most compact form for the net energy change, and it does not clearly show the separate contributions from the electron cyclotron maser interaction, the peniotron interaction, and other interactions. A more compact form can be obtained by combining and re-arranging the terms in $\alpha_1 + \alpha_2 + \alpha_3 + \alpha_4$. To start off with, we will re-write $\langle \delta\gamma \rangle_{t_o \varphi_o}$ in the form

$$
\langle \delta\gamma \rangle_{t_o \varphi_o} = \frac{E_o^2 \gamma_o \omega^2}{k_z^2 U_{z_o}^2 k_\perp^2} \sum_\Gamma \sum_\Lambda A_\Gamma^{I*} A_\Lambda^I \sum_{s=-\infty}^{\infty} \left\{ \left[\frac{s\Omega}{\gamma_o \omega} T_{\Gamma\Lambda s} - \frac{k_\perp U_{\perp_o}}{\gamma_o \omega} U_{\Gamma\Lambda s} \right] \mathcal{G} \right.
$$

$$
+ \frac{2\lambda k_z U_{\perp_o}^2}{\gamma_o U_{z_o} \omega} H_{\Gamma\Lambda s} \mathcal{G} - \frac{U_{\perp_o}^2}{\gamma_o U_{z_o} k_z \omega} \left[\omega^2 - k_z^2 \lambda^2 \right] H_{\Gamma\Lambda s} \mathcal{G}'
$$

$$
\left. + i \frac{k_z L_z}{4\omega} \left[\frac{U_{\perp_o}^2 k_z}{\gamma_o U_{z_o}} H_{\Gamma\Lambda s} + \frac{k_z U_{z_o}}{\gamma_o} T_{\Gamma\Lambda s} \right] \right\}, \tag{99}
$$

where

$$
\lambda = \left(\frac{s\Omega}{\gamma_o} - \omega \right) \frac{\gamma_o}{k_z U_{z_o}}, \tag{100}
$$

$$
\mathcal{G} = \frac{e^{-i[l\pi\lambda + (l-1)\pi]} + 1}{2 (\lambda^2 - 1)^2} - i \frac{l\pi\lambda}{4 (\lambda^2 - 1)}. \tag{101}
$$

While (99) shows explicitly the rapid variations in the magnetic mistuning variable λ about the harmonic resonances, one can still obtain a simpler form for $\langle \delta\gamma \rangle_{t_o\, \varphi_o}$. Upon expanding and re-writing the $H_{\Gamma\Lambda s}$, $T_{\Gamma\Lambda s}$, and $U_{\Gamma\Lambda s}$ terms, the following final expression can be obtained

$$\langle \delta\gamma \rangle_{t_o\, \varphi_o} = -\frac{E_o^2 \gamma_o \omega^2}{k_z^2 U_{z_o}^2 k_\perp^2} \sum_{s=-\infty}^{\infty} \sum_\Gamma A_\Gamma^{I\,*} D_{\Gamma s}^* \sum_\Lambda A_\Lambda^I D_{\Lambda s}$$

$$\left\{ \frac{U_{\perp_o}^2 J_s'^2(K_{L_o})}{\gamma_o U_{z_o}} \left(\frac{\omega}{k_z}\frac{dg(\lambda)}{d\lambda} - \frac{k_z}{\omega}\frac{d\lambda^2 g(\lambda)}{d\lambda} \right) \right.$$

$$- 2s J_s'(K_{L_o}) \left(\frac{s J_s(K_{L_o})}{K_{L_o}}\frac{s\Omega}{\gamma_o\omega} - \frac{k_\perp U_{\perp_o}}{\gamma_o\omega} J_s(K_{L_o}) \right) g(\lambda)$$

$$- \frac{k_\perp^2 U_{\perp_o}^2}{2\gamma_o \Omega \omega} \left[J_{s+1}'^2(K_{L_o}) g(\lambda^+) - J_{s-1}'^2(K_{L_o}) g(\lambda^-) \right]$$

$$- i\frac{k_z L_z}{4}\left[\frac{U_{\perp_o}^2 J_s'^2(K_{L_o})}{\gamma_o U_{z_o}}\left(\frac{\omega}{k_z}\frac{df(\lambda)}{d\lambda} - \frac{k_z}{\omega}\frac{d\lambda^2 f(\lambda)}{d\lambda} + \frac{k_z}{\omega} \right) \right. \tag{102}$$

$$- 2s J_s'(K_{L_o}) \left(\frac{s J_s(K_{L_o})}{K_{L_o}}\left[\frac{k_z U_{z_o}}{\gamma_o\omega}(\lambda f(\lambda) - 1) + f(\lambda) \right] - \frac{k_\perp U_{\perp_o}}{\gamma_o\omega}J_s(K_{L_o}) f(\lambda) \right)$$

$$- \frac{k_\perp U_{\perp_o}}{2\gamma_o \Omega \omega} \left[k_\perp U_{\perp_o}\left(J_{s+1}'^2(K_{L_o}) f(\lambda^+) - J_{s-1}'^2(K_{L_o}) f(\lambda^-) \right) \right.$$

$$\left. \left. \left. + k_z U_{z_o}\left(J_{s+1}(K_{L_o}) J_{s+1}'(K_{L_o}) + J_{s-1}(K_{L_o}) J_{s-1}'(K_{L_o}) + 2 J_s(K_{L_o}) J_s'(K_{L_o}) \right) \right] \right] \right\},$$

where

$$g = \left(\frac{\cos(\mu)}{(\lambda^2 - 1)} \right)^2, \tag{103}$$

$$f = \frac{\lambda}{(\lambda^2 - 1)} + \frac{4\sin(\mu)\cos(\mu)}{k_z L_z (\lambda^2 - 1)^2}, \tag{104}$$

$$\lambda^\pm = \left(\frac{(s \pm 1)\Omega}{\gamma_o} - \omega \right)\frac{\gamma_o}{k_z U_{z_o}}, \tag{105}$$

$$\mu = l\pi\lambda/2 + (l - 1)\pi/2. \tag{106}$$

As the product $\sum_\Gamma A_\Gamma^{I\,*} D_{\Gamma s}^* \sum_\Lambda A_\Lambda^I D_{\Lambda s}$ is real, and since all of the variables and functions within the brackets $\{\ldots\}$ are real, the first set of terms in (102) give the real part

of $\langle\delta\gamma\rangle_{t_o\,\varphi_o}$, and the second set of terms multiplied by i give the imaginary part of $\langle\delta\gamma\rangle_{t_o\,\varphi_o}$. As is shown below, $\mathrm{Re}\big(\langle\delta\gamma\rangle_{t_o\,\varphi_o}\big)$ and $\mathrm{Im}\big(\langle\delta\gamma\rangle_{t_o\,\varphi_o}\big)$ respectively determine the gyrotron start oscillation beam power and resonant frequency detuning. Averaging over the guiding center angle ψ_{gc_o} for a cylindrical cavity or over x_{gc_o} for a rectangular cavity again leads to a reduction of the double sum over cavity eigenfunctions to a single sum. After averaging the product $\sum_\Gamma A_\Gamma^{I\,*} D_{\Gamma_s}^* \sum_\Lambda A_\Lambda^I D_{\Lambda_s}$ is replaced by $\sum_\Gamma |A_\Gamma^I|^2 |\mathcal{E}_{\Gamma_s}|^2$, where $|\mathcal{E}_{\Gamma_s}|^2$ is either $[C_{\Gamma-k}^I]^2$ (or $[J_{\Gamma-k}^I]^2$ if $r_{L_o} > r_{gc_o}$) or $[\cos(k_{y_\Gamma}y_{gc_o})^2\cos(s\lambda_\Gamma)^2 + \sin(k_{y_\Gamma}y_{gc_o})^2\sin(s\lambda_\Gamma)^2]/2$ respectively for cylindrical and Cartesian geometries. The smooth walled limit of equation (102) is obtained by taking the limit $w \to 0$ or $\theta_o \to 0$ in the dispersion relation, and by using $\Gamma = m$, $A_\Lambda^I\delta_{\Lambda\Gamma} = 1$, $A_0^{II} = 0$.

The full behavior of $\langle\delta\gamma\rangle_{t_o\,\varphi_o}$ is clearly given by equation (102). The guiding center dependence is given by the factor $\sum_\Gamma A_\Gamma^{I\,*} D_{\Gamma_s}^* \sum_\Lambda A_\Lambda^I D_{\Lambda_s}$; the resonance behavior as a function of magnetic field about the cyclotron harmonics is given by the functions g and f; and the several interactions which simultaneously take place in a gyrotron are explicitly separated. Cyclotron maser and Weibel emission resonances are given by the terms in $U_{\perp_o}^2 J_s'^2/\gamma_o U_{z_o}(\ldots)$. The terms in $2sJ_s'(\ldots)$ are due to cyclotron maser absorption. Peniotron emission and absorption resonances are represented respectively by the terms with the factors $g(\lambda^-)$, $f(\lambda^-)$, $g(\lambda^+)$, and $f(\lambda^+)$. We note that equation (102) for a smooth walled cylindrical cavity is equivalent to the relation derived by Brand [23], and that the real portion of $\langle\delta\gamma\rangle_{t_o\,\varphi_o}$ averaged over ψ_{gc_o} is in the same form given previously by Vitello [24]. For slotted cylindrical oscillators, the real part of equation (102) can also be shown to equal the more complicated relation by Chu and Dialetis [11–12].

The start oscillation beam power and the frequency detuning equation for steady state operation for any TE$_{mnl}$ mode can be found directly from $\langle\delta\gamma\rangle_{t_o\,\varphi_o}$. Taking the unperturbed beam energy to be P_b, the total net energy transferred from the beam

to the cavity fields is given by $P_b\langle\delta\gamma\rangle_{t_o\,\varphi_o}/(\gamma_o - 1)$. Quite generally [25], the starting power can be given by

$$\overline{Q P_b} = -8.6 \times 10^6 \mathcal{W}(\gamma_o - 1)/\mathrm{Re}\big(\langle\delta\gamma\rangle_{t_o\,\varphi_o}\big)\ \mathrm{kW}, \qquad (107)$$

and the frequency detuning due to the presence of the beam is

$$\frac{\omega - \omega_o}{\omega_o} = -\frac{1}{2Q}\frac{\mathrm{Im}\big(\langle\delta\gamma\rangle_{t_o\,\varphi_o}\big)}{\mathrm{Re}\big(\langle\delta\gamma\rangle_{t_o\,\varphi_o}\big)}, \qquad (108)$$

where $\omega_o = \big(k_\perp^2 + k_z^2\big)^{1/2}$ is the cold cavity frequency. For gyrotron tubes, the quality factor Q is due mainly to diffractive losses, and with a good estimate of its value obtained from cold cavity tests (107) provides an good estimate of the actual start oscillation power required. By contrast, the linear theory values for the frequency detuning often differ significantly from the detuning under normal high field operating conditions [23] and should used with caution. Again we stress that for $r_{L_o} > r_{gc_o}$ there must be a replacement in the above relations of $\mathcal{C}^I \to J$ and $J \to \mathcal{C}^I$.

IV. Discussion

We have extended the modeling of the linear kinetic theory for gyrotron oscillators to cavities with slotted rectangular and cylindrical co-axial cross sections. The averaged beam perturbed energy change is shown in a form (102) which is the same in rectangular and cylindrical cavities. The cavity geometry determines only $k_\perp$ and the magnitude of each harmonic contribution to the overall RF cavity field of a particular mode. For each harmonic, the functional form of the differing interactions, such as the electron cyclotron maser and the peniotron interactions, do not vary with the cavity geometry and are the same for smooth walled and slotted tubes. Studies of the relative strengths of the interactions for smooth walled gyrotrons [25] can therefore be applied directly to slotted cavity devices.

We apply here our results to the slotted rectangular and cylindrical cavities discussed earlier. In the case of a cylindrical cavity we set $R_i = 0$, average $\langle \delta\gamma \rangle_{t_o \, \varphi_o}$ over ψ_{gc_o}, and use an axis encircling electron beam to allow for comparison with the results of Chu and Dialetis [11–12]. In Figure 3 we show the E_θ RF field profile for the TE_{311} mode for a cavity with $N = 6$ and $R_o = 1.4$. As one of the major advantages of the slotted cylindrical cavity is the reduction of the start oscillation condition with increasing R_o, we plot QP_b in Figure 4 for both the electron cyclotron maser interaction and the peniotron interaction as a function of R_o. In the figure, L_z is increased with increasing R_o to hold $k_\perp/k_\parallel$ fixed at 10.7. The decrease in QP_b with R_o is partially due to the effects of a longer cavity, but is primarily caused by the increasing slot depth. The electron cyclotron maser emission curve for 49.9 KeV is terminated at the R_o value where the Larmor radius strikes the cavity wall. Our results for the electron cyclotron maser QP_b are in agreement with Chu and Dialetis. However, we find that at low beam energy the start oscillation condition is actually *smaller* for the peniotron interaction. Chu and Dialetis give results only for the electron cyclotron maser resonances and do not consider the peniotron resonances.

As an example of the effect of slots in a rectangular cavity gyrotron oscillator we will consider the start oscillation condition QP_b for the cavity and beam parameters investigated by Han and Ferendeci [17] for a slotted rectangular cavity gyro-TWT. For the TE_{021} mode, which Han and Ferendeci found to give strong sixth harmonic emission, we place the electron beam in Region I at $x_{gc_o} = L_x/2$, $y_{gc_o} = R/2$. Figure 5 shows the E_x component of the RF field. The strong fringe field observed in this figure couples very strongly with high harmonic emission. This coupling will be significant at high harmonics since with rising harmonic number s the growth of the the Larmor radius, $r_{L_o} \simeq s\beta_{\perp_o}/\omega$, allows the beam to increasingly penetrate the fringe fields. In Figure 6 we show QP_b for the slotted rectangular cavity as a function of magnetic field for multiple harmonic emission. Harmonics greater than the sixth are not shown as the beam Larmor radius would be greater that one-half the cavity width R. For comparison QP_b for a smooth walled rectangular cavity is shown also. For our beam position, the smooth walled cavity only shows emission at the even harmonics. For the slotted cavity, harmonics for $s = 1$-3 are dominated by the electron cyclotron maser instability. The fourth harmonic is due primarily to the peniotron instability. For harmonics greater than fourth, both the electron cyclotron maser and peniotron instabilities strongly contribute. It is evident that the addition of slotted not only enormously enhances the very high harmonic ($s > 4$) interaction and hence greatly lower QP_b, but this enhancement *increases* with increasing harmonic number. This decrease in QP_b with harmonic number is implicit also in the ridged gyro-TWT modeling of Han and Ferendeci. For the smooth walled rectangular, smooth walled cylindrical, or even ridged cylindrical cavities with axis encircling beam previously studied in the literature, the standard behavior with increasing harmonic number is a growth in the start oscillation beam power. The high harmonic interaction observed here for the ridged rectangular cavity shows a great potential for the practical development of a high frequency, low magnetic field gyrotron oscillator.

In conclusion we find that for complex cross gyrotron cavities the start oscillation condition can be written in a form which separates the geometric factors from the physical interaction terms. An analysis of slotted cavities using this formalism shows that slots can be used to enormously enhance the high harmonic RF field, beam interaction for both rectangular and cylindrical cavities, and for both the fundamental electron cyclotron maser and the peniotron interactions.

References

[1] J.M. Baird, "Survey of fast wave tube developments," *Tech. Dig. Int. Electron Devices Meet.*, pp. 156–163, 1979.

[2] R.S. Symons & H.R. Jory, "Cyclotron resonance devices," in *Advances in Electronics & Electron Physics*, L. Marton & C. Marton, Eds., vol. 55, New York: Academic, pp. 1–75, 1981.

[3] V.L. Granatstein, M. Read, & L.R. Barnett, "Measured performance of gyrotron oscillators and amplifiers," *Int. J. Infrared Millimeter Waves*, vol. 5, pp. 267–304, 1984.

[4] D.B. McDermott, N.C. Luhmann, Jr., & D.S. Furuno, "Operation of a high-harmonic gyrotron," *Eighth Int. Conf. Infrared Millimeter Waves*, TH4.1, 1983.

[5] D.B. McDermott & N.C. Luhmann, Jr., "Operation of a compact mm-wave high-harmonic gyrotron," *Proc. SPIE*, vol. 423, pp. 58–63, 1983.

[6] W.W. Destler, R.L. Weiler, & C.D. Striffler, "High power microwave generation from a rotating e-layer in a magnetron-type waveguide," *Appl. Phys. Lett.*, vol. 38, pp. 570–572, 1981.

[7] Y.Y. Lau & L.R. Barnett, "Theory of a low harmonic field gyrotron (Gyromagnetron)," *Int. J. Infrared Millimeter Waves*, vol. 3, pp. 619–744, 1982.

[8] P.S. Rha, L.R. Barnett, J.M. Baird, & R.W. Grow, in Int. Electron Device Meet., pp. 525–538, 1985.

[9] R.W. Grow & U.A. Shrivastava, "Impedance calculations for traveling wave gyrotrons operating at harmonics of the cyclotron frequency in magnetron-type circuits operating at the PI mode," *Int. Electron Devices Meet.*, pp. 384–387, 1982.

[10] H.S. Uhm, C.M. Kim, & W. Namkung, "Theory of cusptron microwave tubes," *Phys. Fluids*, vol. 27, pp. 488–498, 1984.

[11] K.R. Chu & D. Dialetis, "Theory of harmonic gyrotron oscillator with slotted resonant structure," *Int. J. Infrared Millimeter Waves*, vol. 5, pp. 37–56, 1984.

[12] K.R. Chu & D. Dialetis, "Kinetic theory of harmonic gyrotron oscillator with slotted resonant structure," *Infrared Millimeter Waves*, vol. 13, pp. 45–74, 1985.

[13] J.Y. Choe & W. Namkung, "Experimental results of cusptron microwave tube study," *IEEE Trans. Nuclear Sci.*, vol. NS-32, pp. 2882–2884, 1985.

[14] U.A. Shrivastava, R.W. Grow, P.S. Rha, J.M. Baird, & L.R. Barnett, "Threshold power transfer for the gyrotron and peniotron oscillators operating at the harmonic cyclotron frequencies using coaxial electron beam-circuit configurations," *Int. J. Electron.*, vol. 61, pp. 33–59, 1986.

[15] P. Vitello, *Eleventh International Conf. Infrared Millimeter Waves*, Tirrenia, Pisa, Italy, pp. 46–48 (1986).

[16] A.M. Ferendeci & C.C. Han, "Theory of high-harmonic rectangular gyrotron for TE_{mn} modes," *IEEE Trans. Electron Devices*, vol. ED-31, pp. 1212–1218, 1984.

[17] C.C. Han & A.M. Ferendeci, "Nonlinear analysis of a high-harmonic rectangular gyrotron," *Int. J. Electron.*, vol. 57, pp. 1055–1063, 1984.

[18] A.M. Ferendeci & C.C. Han, "Linear analysis on an axially grooved rectangular gyrotron for harmonic operation," *Int. J. Infrared Millimeter Waves*, vol. 6, pp. 1267–1282, 1985.

[19] Q.F. Li & J.L. Hirshfield, "Gyrotron traveling wave amplifier with out-ridged waveguide," *Int. J. Infrared Millimeter Waves*, vol. 7, pp. 71–98, 1986.

[20] J. D. Jackson, Classical Electrodynamics, (John Wiley & Sons, Inc., New York, 1962).

[21] G. B. Collins, *Microwave Magnetrons*, (McGraw-Hill, New York, 1948).

[22] M. Abramowitz & A. Stegun, Handbook of Mathematical Functions, (Dover Publications, Inc., New York, 1972).

[23] G.F. Brand, "A gyrotron frequency detuning equation," *Int. J. Infrared Millimeter Waves*, vol. 4, pp. 919–931, 1983.

[24] P. Vitello & K. Ko, "Mode competition in the gyro-peniotron oscillator," *IEEE Trans. Plasma Sci.*, vol. PS-13, pp. 454–463, 1985.

[25] P. Vitello, W.H. Miner, & A.T. Drobot, "Theory and numerical modeling of a compact, low-field, high-frequency gyrotron," *IEEE Trans. Microwave Theory Tech.*, vol. MTT-32, pp. 373–386, 1984.

Figure Captions

Figure 1a. Cross-section of the slotted cylindrical gyrotron.

Figure 1b. Cross-section of the slotted rectangular gyrotron.

Figure 2. Guiding center coordinate system.

Figure 3. E_θ RF field for a ridged cylindrical cavity with $R_o = 1.4$, $\theta_o = \pi/2N$, $N = 6$.

Figure 4. Variation of the start oscillation condition for the third harmonic electron cyclotron maser interaction (dashed curves) and second harmonic peniotron interaction (solid curves) as a function of R_o for the TE_{311} mode. The beam axial velocity is $\beta_{z_o} = 0.1$.

Figure 5. E_x RF field for a ridged rectangular cavity with $L_x = 2.186$, $R_o = 1.198$, $w = 0.05466$, and $N = 3$.

Figure 6. TE_{021} mode start oscillation condition for the rectangular cavity for the electron beam with 72 keV, and $\beta_{z_o} = 0.28$. The solid curve gives QP_b for the ridged cavity, while the dashed curve gives QP_b for the smooth walled cavity.
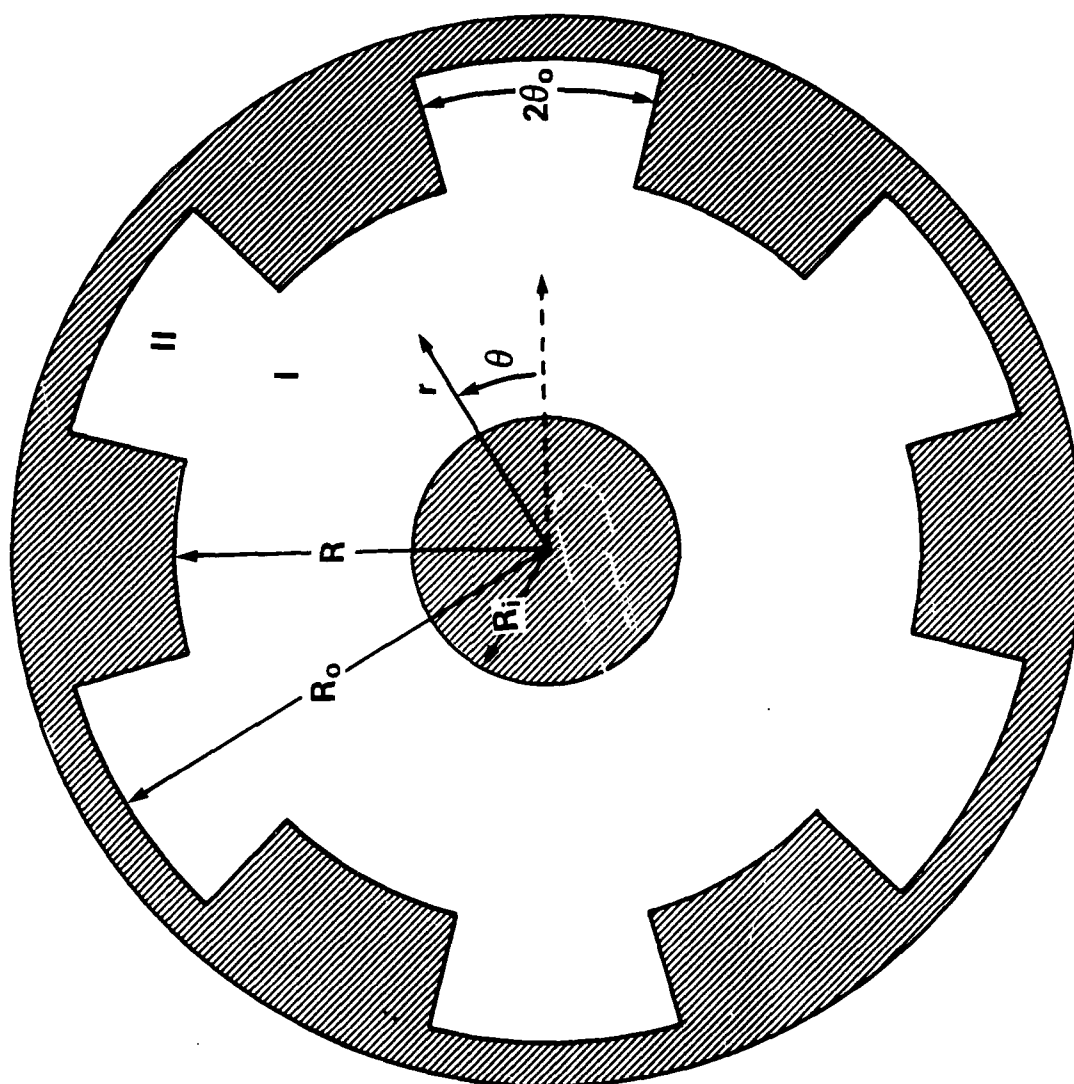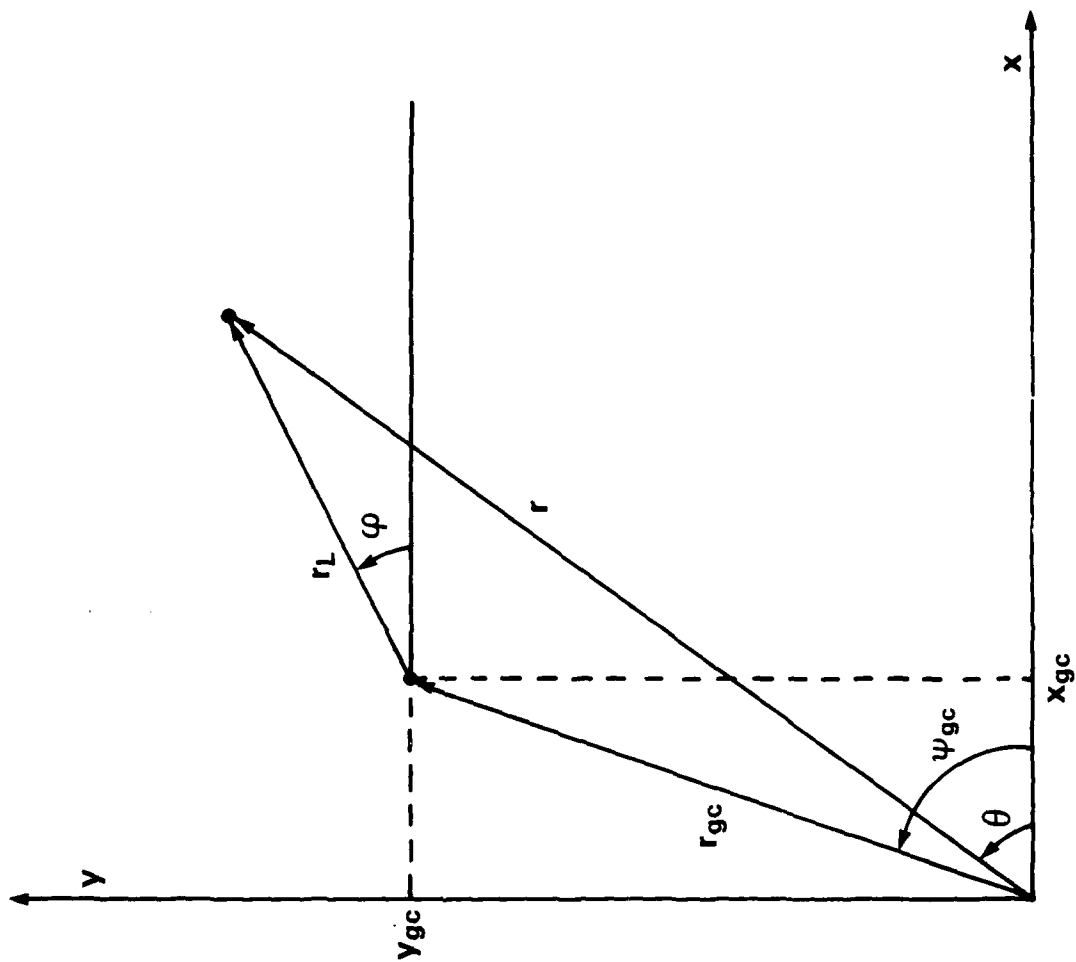
FIGURE 1a
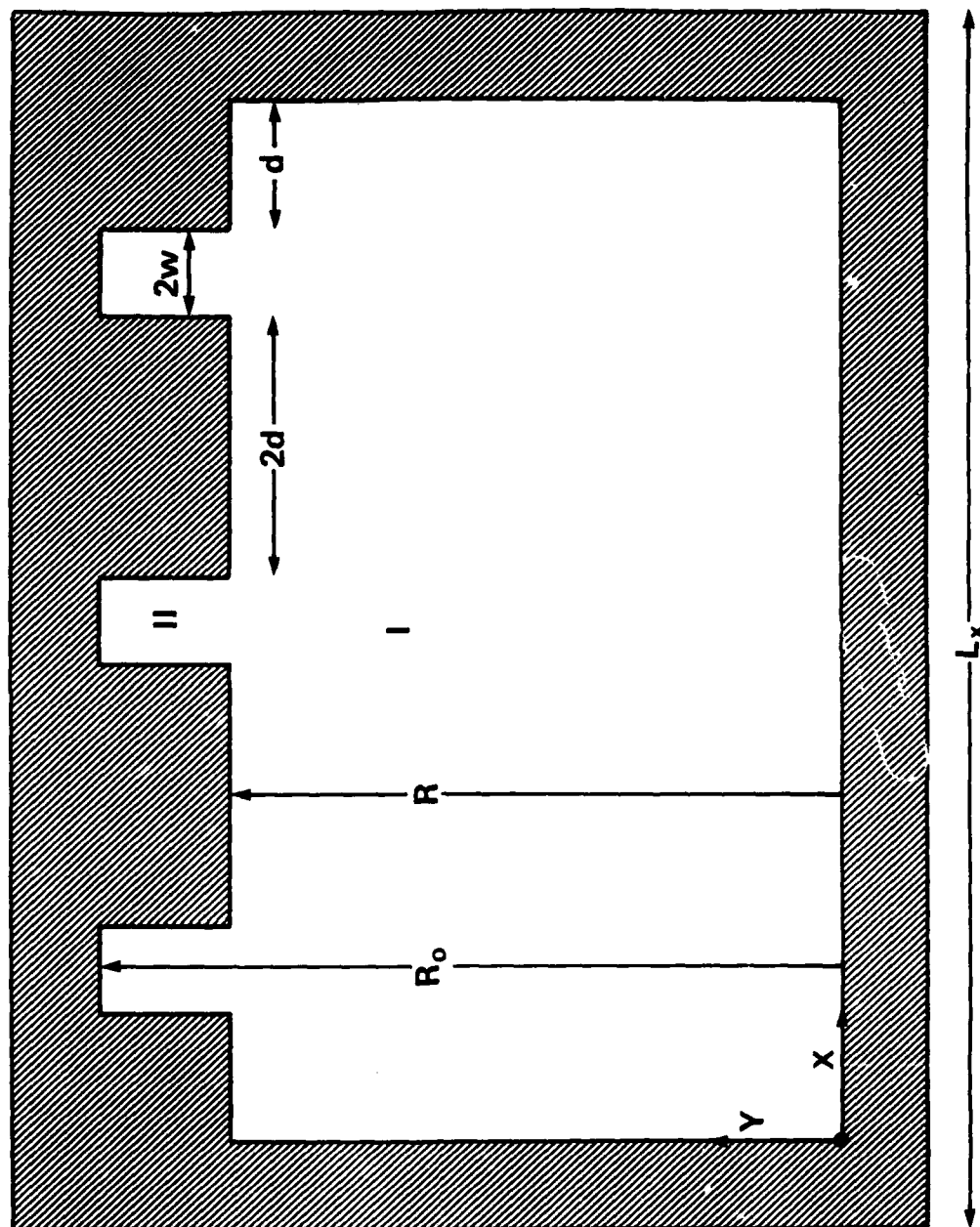
FIGURE 1b

FIGURE 2

TE_{311}
$E_{max} = 5.305*10^{-1}$
$k_{\perp} = 2.072$
$W_R = 5.433*10^{-3}$
$W_T = 9.856*10^{-3}$
$\theta_o = 2.618*10^{-1}$
$R_o = 1.400$

Figure 3

80

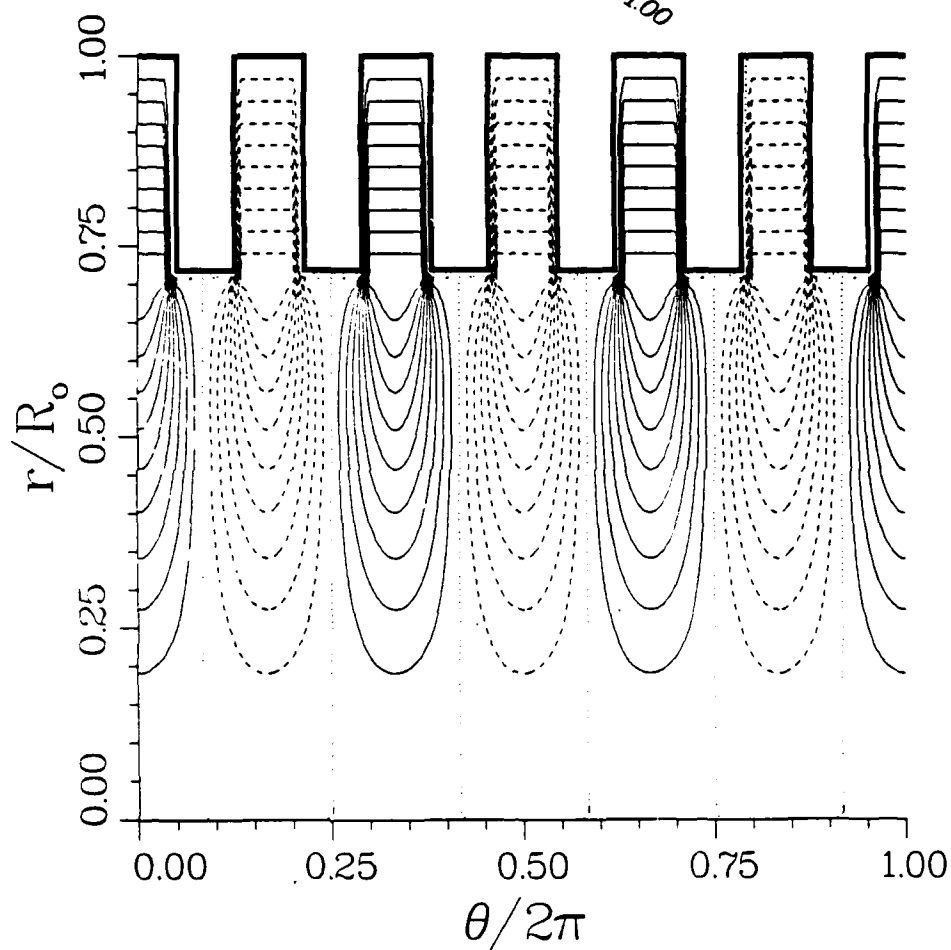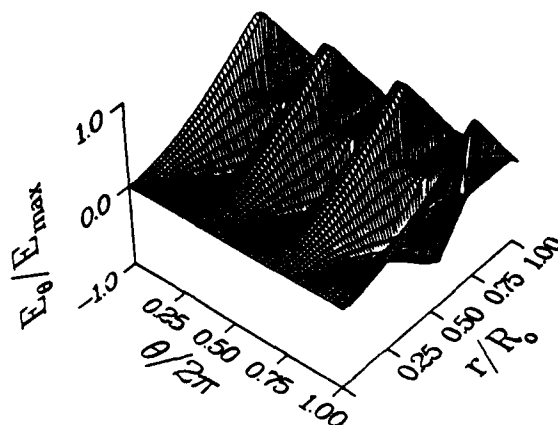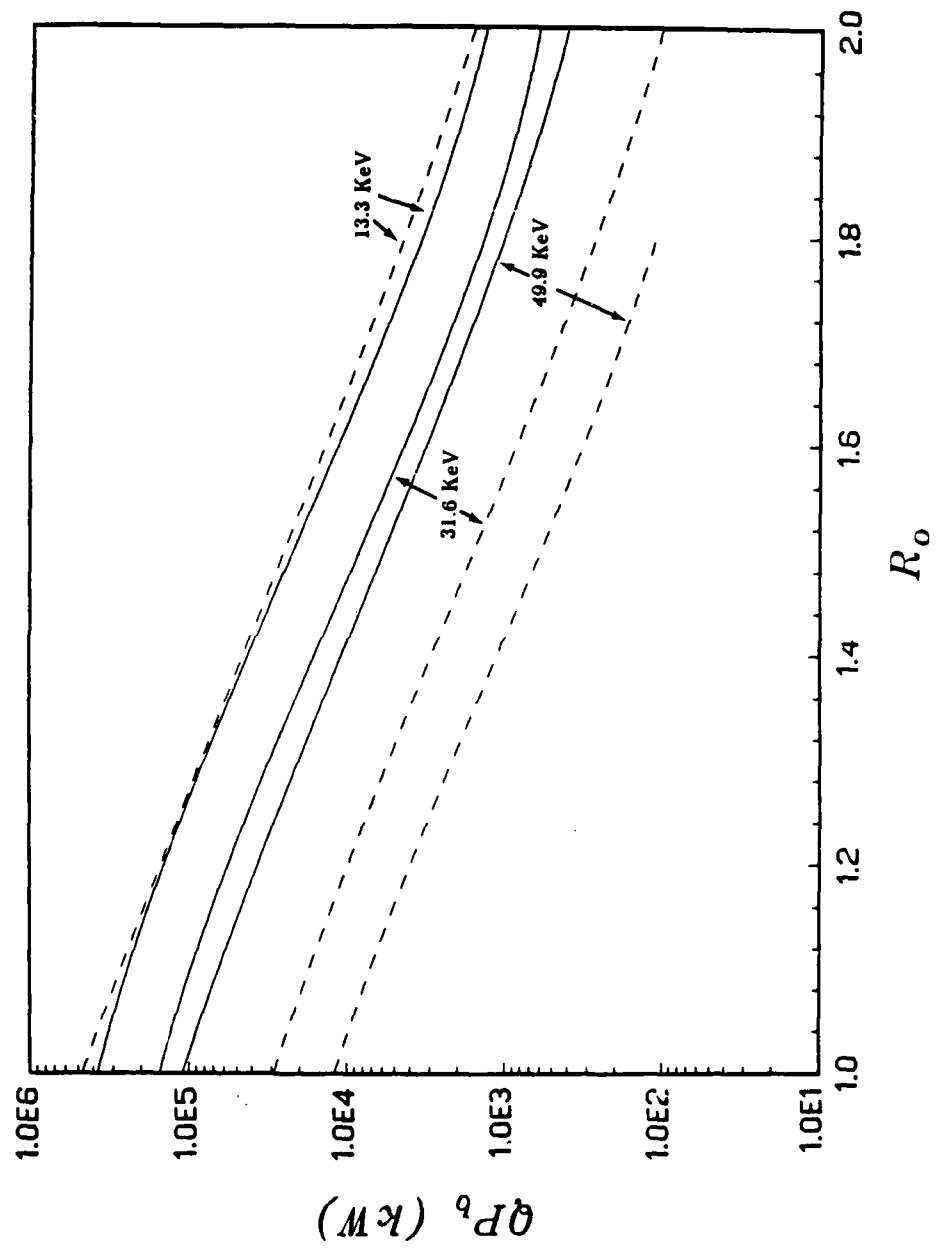Figure 4

TE$_{021}$

$E_{max} = 4.108*10^0$

$k_\perp = 5.522$

$L_x = 2.186$

$R_o = 1.198$

$w = 5.466*10^{-2}$

$W_R = 1.325*10^{-2}$

$W_T = 3.498*10^{-2}$

Figure 5

Figure 6